1 From analytical methods to numerical simulations: a process engineering

2 toolbox for 3D-concrete printing

- 3 A. Perrot¹, A. Pierre², V.N. Nerella³, R. J. M. Wolfs⁴, E. Keita⁵, N. Neithalath⁶, N. Roussel⁵, V.
- 4 Mechtcherine⁴
- 5 ¹ Univ. Bretagne-Sud, UMR CNRS 6027, IRDL, F-56100 Lorient, France
- 6 ²L2MGC, EA4114, CY Cergy Paris Université, Cergy-Pontoise, France
- 7 ³ Institute of Construction Materials, Technische Universität Dresden, 01062 Dresden,
- 8 Germany
- 9 ⁴ Department of the Built Environment, Eindhoven University of Technology, Netherlands
- ⁵ Laboratoire Navier, UMR 8205, École des Ponts, CNRS, UGE, Champs-sur-Marne, France
- 11 ⁶ Arizona State University, Tempe, USA

12 13

14

Abstract

- 15 This paper compiles selected predictive analytical and numerical tools which can be used to
- model and understand the mechanisms of importance at different stages during and immediately
- 17 after extrusion-based 3D printing of cementitious materials. The proposed toolbox covers
- different aspects of the process including mixing, material transportation, layer deposition,
- mechanical behavior of the fresh printed structure, and its early curing. Specifically, the paper
- 20 provides basic analytical methods that should be helpful for an initial, first-order analysis of a
- 21 given printing process. These methods deliver, in turn, a first estimation of some material
- 22 requirements and process parameters. Limitations of these analytical methods are also
- 23 discussed. Furthermore, the paper presents a review of advanced numerical tools that can be
- 24 used to simulate the steps in the printing process accurately. It is shown that these tools can
- 25 serve to describe complex behaviors, help in designing process parameters, or optimizing the
- 26 rheological response, even though further developments are still needed to capture fully the
- 27 attendant physical mechanisms.

28

31

- 29 Keywords: Concrete technology; additive manufacturing; 3D-printing; analytical modeling;
- 30 numerical simulations

1. Introduction

- 32 In the last decade the potential of 3D concrete printing in the construction industry has been
- widely reported in the media. In 2017 CNN on its website posed the question "Will the world's
- 34 next megacity drip out of a 3D printer?". However, despite ubiquitous media coverage it is
- important to recognize that we have barely left the period of "demonstrators"; currently,
- digitally manufactured concrete in both academia and industry are mostly produced without
- 37 regard to cost, effort, and resources. Field implementations to date have mainly showcased the
- 38 potential of the technology by demonstrating that a building component or even a house can be
- 39 produced using automated digital technologies.
- 40 There is, however, a strong sense of anticipation in the construction industry, fueled by the
- 41 international recognition of the need for wider automation of construction [1,2]. Several
- 42 specialist companies have emerged, and startup initiatives are proliferating. At the beginning

43 of 2013 there were 20 startups in the field. Five years later, there were more than 65 of them 44 offering services, tools, building components, or even entire buildings. In parallel several large, 45 well established companies in Europe have taken the decision to adopt this technology early on, have made strategic moves, and have started acquiring specialized skills and capabilities in 46 47 robotics. Finally, regulation and numerous public policy measures are encouraging the adoption 48 of 3D concrete printing (3DCP) in many parts of the world such as the Middle East, the United 49 Kingdom, China, with its own draft of a national standard for 3D concrete printing, and the U.S. The Boston Consulting Group concluded in its 2018 report that "As this evolution 50 51 proceeds, the construction industry as a whole will be transformed. Companies and 52 governments would do well to prepare for this transformation and to influence it as far as 53 possible to their own advantage"[3].

54

55

56

57

58 59

60

61

62

63

64

65

66 67

68

69

70

71

72

73 74

75

76 77

78

79

80

81 82

83

84

85

86

87

Most applications and demonstrators are based on extrusion, where a mineral-based, often cement-based, material is extruded to form sequential layers via a digitally controlled nozzle mounted on a robotic arm, gantry, or crane. The processes are similar to conventional additive manufacturing processes except that the material characteristics and scale of manufacture give rise to unique challenges and questions: the formulation of mixtures that can be pumped and still be, once placed, stable in shape, can provide reliable interlayer bonding, and are controllable in respect of curing the material. The application of 3DCP components also suggests further questions with respect to durability, structural reinforcement, quality control, design, and production logistics.

The outlook, however, is very promising. It is anticipated that 3D concrete printing will become competitive with conventional in-situ and off-site construction if the existing technological obstacles can be overcome and if engineers with the relevant skills and knowledge support the integration of such novel processes within the industry. The degree of importance of these obstacles varies significantly depending on the application and its technology's degree of readiness. However, to implement such transformations successfully in a relatively traditional industry, the exchange of knowledge between academia and industry must not be left behind.

In Zurich in 2018 [4] and Eindhoven in 2020 [5] following the two first RILEM international conferences on digital fabrication with concrete, it is now possible comprehensively to lay out the global state-of-the-art knowledge. What is apparent is that the number of published papers is exploding, various academic groups are dealing with transdisciplinary questions, and the diversity of the technologies under study is impressive. What has grown out of this is a dynamic, diverse, and multi-disciplinary scientific community. Moreover, it also brings with it a large number of scientific articles published in many different journals and dealing with the increasingly varied aspects of 3DCP.

This paper aims at compiling and organizing the fundamental principles and their representations, allowing for the assessment of the 3D printing process as a function of its material properties, the object's geometry, and the printing parameters. The intent here is to provide a comprehensive toolbox for the engineer to facilitate an a priori assessment/prediction of the salient features of the material to be used in the specific application. This paper also details the limitations of these first order principles and provides, when available, references to more advanced numerical tools still under development. The paper is organized in a sequence parallel to an actual construction process, starting with mixing, moving on to transportation. i.e., pumping and extrusion, treating in turn the placement and stability of the in-print structure, and examining the early-age development of the material's characteristics.

2. Analytical methods

2.1 Mixing

88

- 90 In concrete 3D printing processes, the mixing step is critical in ensuring that the printed final
- 91 component/structure exhibits the desired properties. It has, for example, been shown that the
- 92 mechanical properties of cementitious materials depend on the energy of mixing [6,7].
- 93 Moreover, high-shear mixing can induce the crushing of solid particles, which can lead to
- 94 enhanced structural build-up rates in the fresh state, thus proving useful in ensuring global
- 95 stability of the printed system at early ages [8]. However, a high level of process control is
- 96 required to enable this.
- Many printing methods involve the incorporation of a chemical admixture in the printhead just
- before material deposition in order to allow a rapid printing process [9]. The added product can
- be an accelerator that speeds up the formation of hydrated products or a flocculent that promotes
- the formation of colloidal particle bonds. The binder itself can be chemically different, e.g., an
- aluminate-based binder capable of rapidly setting [10]. In such situations in the printhead, the
- quality of the dispersion depends on the material's time of residence there, which ranges
- between 1 s and 100 s, as explained by Wangler et al. [11]. In order to ensure homogeneous
- dispersion of the admixture in the printhead, a mixing system either static or rotating is
- required [9]. This can be explained by the Stokes-Einstein theory, which predicts a typical
- diffusion length L_D of less than a few hundredths of a micrometer, expressed as the square root
- of the product of the diffusion coefficient of the accelerator and the residence time $(D_{mix}.t_{res})^{0.5}$.
- 108 The diffusion coefficient can be computed using the following equation:

$$109 D_{mix} = \frac{kT}{6\pi r_{acc}\mu} (1)$$

- Where k is the Boltzmann constant, T is the temperature, r_{acc} is the radius of the admixture
- molecule, and μ is the apparent viscosity of the cementitious material. According to
- Mechtcherine et al. [9], the mixing system must be able to create sheared layers that must be
- spaced at a distance smaller than L_D in order to ensure homogeneous dispersion for a fixed
- 114 residence time.
- In practice, the mixing kinetics are often assessed using a Wattmeter that measures the time
- evolution of the electrical energy consumption of the mixer. However, the recording of the
- power consumption provides noisy data [12,13] that, even if it asymptotically tends to a steady-
- state plateau value, is not sufficient to guarantee the homogeneity of the material [14]. Using
- tracer particles in colorimetric index measurement, Jézéquel and Collin [14] described the
- dispersion during the mixing process. They showed that the colorimetric index of the tracer
- particles tends to a plateau value representative of the homogeneous material after following an
- exponential kinetic law.

$$c = c_{plateau} + (c_0 - c_{plateau}) \exp\left(\frac{-t}{t_c}\right)$$
(2)

- Where $c_{plateau}$ is the final colorimetric index, c_0 is the initial value and t_c is the characteristic
- dispersion time. Note that the characteristic time considers different mechanisms such as
- crushing, erosion and diffusion. The characteristic time has been shown to depend on the
- mixer's speed Ω according to the following equation:

$$128 t_c = \left(\Omega(\alpha\Omega - \beta)\right)^{-1} (3)$$

- Where α and β are the fitting parameters, β depending on the material's static yield stress. The
- characteristic dispersion time was reported to vary between one and ten minutes.
- Nevertheless, to use this equation, experiments are needed to estimate the fitting parameters for
- the chosen materials and mixers. Mechtcherine et al. [9] noted that printhead mixing systems
- are today designed by trial and error and that numerical simulations are needed for better
- predictions of dispersion of materials during mixing.

2.2 Material delivery

- There are two stages in material delivery in the case of extrusion-based 3D-printing processes.
- While pumping is used to deliver the material from mixer to printhead over a length of many
- meters, extrusion takes place at the printhead.
- 139 2.2.1 Pumping

135

- Even though large-scale pumping experiments with printable concretes have not yet been
- reported, pumpability over long distances is a prerequisite for many onsite projects. Concrete
- pumpability depends on materials and processing parameters, and can be described by the
- pressure-flow rate relationships [15,16].
- 144 Pressure calculations carried out using the traditional Buckingham-Reiner equation for complex
- suspensions such as concrete result in overestimating pumping pressures, often by 2 to 5 times
- 146 [17–19]. This discrepancy is attributed to shear-induced particle migration (SIPM) and resulting
- segregation, along with some water migration, leading to the formation of the so-called
- lubricating layer (LL) at the wall of the pipe. The LL exhibits much lower values of Bingham
- parameters; i.e., yield stress $\tau_{0,i}$ and plastic viscosity $\mu_{i,i}$ in comparison to the bulk concrete which
- forms a plug around the longitudinal axis of the pipe [15,17–20]; see Figure 1. Kaplan *et al.*
- 151 [15] described concrete flow in pipes as slip-flow, when the shear stress τ_i at the concrete-pipe
- [15] described consistent now in pipe as sinp now, when the sheet street the time consistent pipe
- wall interface is lower than the yield stress τ_0 of concrete. Otherwise, slip-plus-shear flow
- 153 occurs.

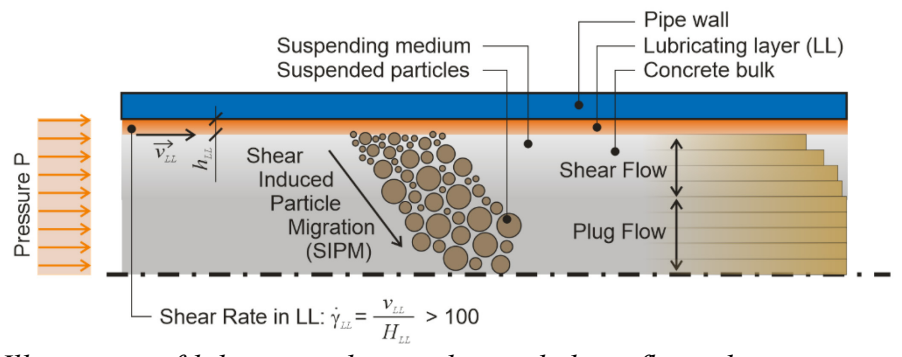


Figure 1: Illustration of lubrication layer, plug and shear flows during concrete pumping indicating flow-induced particle migration. Adapted from [21].

154 Considering the various approaches to 3D concrete printing based on extrusion, different flow

patterns can be expected. Referring to the extremes suggested by Roussel [22], the

implementation of the "infinite brick" approach with the corresponding high yield stress of

printable concrete results in slip/plug flow, while the "free flow" approach is associated with

slip-plus-shear flow in the pipe due to low yield stress of concrete used in such applications

159 [9,22]. Kaplan [23] proposed and validated two analytical models to relate pressure ΔP and

160 flowrate Q_p using Bingham parameters, shear yield stress τ_0 and plastic viscosity μ , for bulk

161 concrete and interface Bingham-like parameters for the lubricating layer; see Eqs. 4 and 5. Eq.

4 is valid in the case of slip/plug flow; the fitting coefficient k can be obtained by means of

tribological measurements [15,24].

$$164 \qquad \Delta P = \frac{2L_{pipe}}{R_{pipe}} \left[\frac{Q_p \mu_i}{\pi R_{pipe}^2 k} + \tau_{0,i} \right] \tag{4}$$

where L_{pipe} is the pipe length and R_{pipe} its radius.

166 Eq. 5 covers the case of slip-plus-shear flow, where the properties of both concrete and LL are

167 considered:

172

178

168
$$\Delta P = \frac{2L_{pipe}}{R_{pipe}} \left[\frac{\frac{Q_p}{\pi R_{pipe}^2 k} - \frac{R_{pipe}}{4\mu} \tau_{0,i} + \frac{R_{pipe}}{3\mu} \tau_0}{1 + \frac{R_{pipe}}{4\mu} \mu_i} \mu_i + \tau_{0,i} \right]$$
 (5)

To determine the rheological properties of concrete and lubricating layer as well as the LL

thickness is a challenging task which limits the applicability of above models for the prediction

of pumping pressures [25–27]. Hence, simplified prediction approaches have been suggested

based on testing devices that mimic pumping procedure to some extent, most prominent of

which is the so-called SLIPER (SLIding Pipe rheometER) device [19]. Such tools and the above

models give rough estimations of pumping parameters; however, their validity has not been

systematically verified for high-yield stress printable concretes as yet. Although pumpability

primarily depends on the plastic viscosity of concrete and LL, the influence of yield stress

increases with increasing τ_0/μ [28]. Pumpability prediction of various printable concretes in

complex pipe geometries and the exact determination of the LL thickness require the use a

multiphase approach and appropriate numerical tools.

180 2.2.2 Extrusion

181 The extrusion of concrete is associated with material flow through the printhead with the section

182 narrowing towards the nozzle exit. The literature dealing with this process step is mainly

inspired by the work of Benbow and Bridgwater [28], initially developed for ceramic forming

to enable the prediction of the additional pressure required to shape the extruded material

exiting through an axisymmetrical nozzle. The corresponding formula for estimating the

extrusion pressure P_{ext} is based on the ideal work theory which links plastic bulk elongational

and interfacial shear yield stresses of the extruded material; see Eq. 6 below:

188
$$P_{ext} = 2(\sigma_0 + a_0 N_{ext}^{n_0}) \ln(\frac{D_{ext}}{d_{die}}) + 4 \frac{L_{die}}{d_{die}} \cdot (\tau_{0,i} + a_1 N_{ext}^{m}))$$
 (6)

Where σ_0 is the elongational yield stress, $\tau_{0,t}$ is the interfacial shear yield stress, d_{die} is the die

diameter, D_{ext} the extruder diameter, V_{ext} the material average velocity, and a_0 and a_1 are

empirical coefficients that are used to describe the flow-rate-dependent behavior of the materials. Assuming axisymmetrical convergent flow, Basterfield *et al.* [29] generalized the theory of Benbow and Bridgwater to make it compatible with Herschel-Bulkley (HB) modeling parameters, see Eq. 7. This formula can be used for predicting extrusion force on the basis of data obtained by rheological measurements.

$$196 \qquad P_{ext} = 2\sqrt{3}\tau_0 \ln\left(\frac{D_{ext}}{d_{die}}\right) + \frac{2\eta\sqrt{3}^{n+1}}{3n \cdot 2^n} \left(\frac{2V_{ext} \cdot D_{ext}^2}{d_{die}^3}\right)^n \sin\theta (1 + \cos\theta)^n \left(1 - \left(\frac{d_{die}}{D_{ext}}\right)^{3n}\right) + 4\frac{L_{die}}{D_{ext}} \left(\tau_{0,i} + a_1 V^m\right)$$

197 (7)

Where τ_0 is the shear yield stress, η is the HB viscosity, n the flow index from the HB model, and θ is the angle of the conical drawn by the convergent flow.

Many authors have adapted the Benbow/Bridgwater or Basterfield *et al.* models to specific cases with particular nozzle geometries in the extrusion of cementitious materials [30–39]. In each of these works, extrusion pressure is a combination of the pressure needed to overcome interfacial friction at the extruder wall and the plastic work needed to reshape the bulk material. Note that all these models assume cylindrical geometry; the development of analytical models of the extrusion pressure for non-axisymmetrical geometries becomes very difficult; thus, numerical simulation becomes necessary.

Furthermore, for complex extruder geometries, determining exact material flow rate Q_e at the outlet of the extruder is an essential task for controlling the 3D printing process. For example, progressive cavity pumps (PCPs) or eccentric screw pumps are the devices most frequently used in extrusion-based 3D concrete printing due to their robustness and precision as well their ability to deliver high viscous granular suspensions. PCPs contain a stator and rotor assembly; they work based on the principle of progressively opening the conveying chambers with the rotor's eccentric motion in the stator. The eccentricity e defines the relative displacement of the rotor center with respect to the center of stator during operation; see Figure 2 [40]. The parameter overlap e can be defined as the algebraic difference of the rotor diameter e and the inner diameter of the stator. Depending on e, the PCPs can be categorized into: a) equal fit PCPs, b) clearance fit PCPs (e0), and c) interference fit PCPs (e0). The interference fit is possible by making the stator's inner walls out of compressible elastomers. The theoretical volumetric flow rate e0 are PCP with a stator pitch e1 can be calculated by multiplying volume of material displaced per rotation (e1 can be calculated by multiplying volume of material displaced per rotation (e2 can be calculated by multiplying volume of material displaced per rotation (e3 can be calculated by multiplying volume of material displaced per rotation (e4 can be calculated by multiplying volume of material displaced per rotation (e4 can be calculated by multiplying volume of material displaced per rotation (e4 can be calculated by multiplying volume of material displaced per rotation (e6 can be calculated by multiplying volume of material displaced per rotation (e6 can be calculated by multiplying volume of material displaced per rotation (e6 can be calculated by multiplying volume of material displaced per rotation (e6 can be calculated by multiplying v

$$222 Q_{pcp} = 4 \cdot e \cdot D_r \cdot P_{st} \cdot n_r (8)$$

A detailed derivation of Eq. 8 can be found in [40]. While Eq. 8 is valid for PCPs, for the cases of clearance fit or interference fit, equations presented in Pessoa *et al.* [41] can be applied.

These analytical relationships have some limitations since they are based on the assumption that the extruded material remains homogeneous. As a result they neglect issues such as liquid drainage [42,43] and blockage of the coarse aggregates [44] related to extrusion-induced heterogeneities that can occur during the 3D printing of cementitious materials. For such cases, dedicated numerical tools, capable of analyzing multiphase flow in extruder need to be developed.

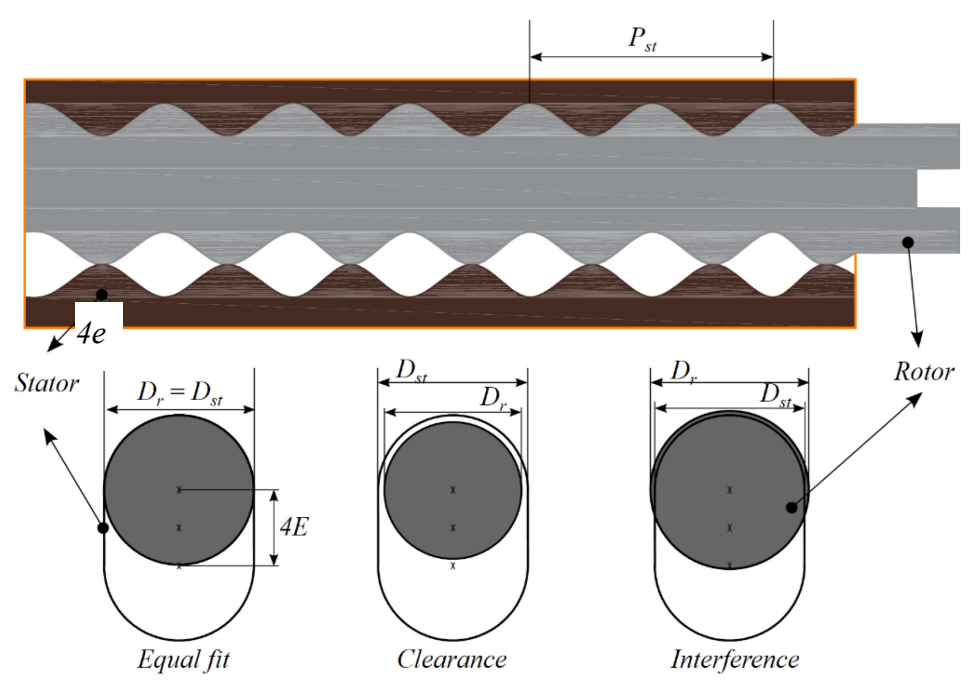


Figure 2: A sectional view of a progressive cavity pump (PCP) geometry. Three cases based on stator and rotor diameters are depicted.

2.3 Material deposit

Material deposition deals with the requirement that the printed layers be deposited in conformance with the targeted geometry. The analytical approach to this problem is limited to the case of linear deposition of a continuous layer of constant height and width. In addition, the material is considered to be isotropic and homogeneous. A deposition strategy ranging between two opposite asymptotic cases can be chosen: the first, "infinite brick extrusion" deposits an unsheared firm material, and the second, "free flow deposition" uses a highly flowable material with the addition of accelerating admixtures just before the deposition [22][45].

For the deposition of the material, simple analytical formulations describing the ability of the material to withstand its own weight and support the pressure of the nozzle can be used as a first approximation [46,47]. Once the material exits the nozzle, the flow ceases if the yield stress of the network of interacting particles is greater than the applied stress. It should be noted here that static yield stress depends on shear history and microstructure build-up, and describes the initiation of the flow, while dynamic yield stress corresponds to the yield stress that develops during the steady-state flow of the material, for example, during pumping [48]. These values differ, and realistic yield stress values depending on the shear profile within the printhead should be chosen according to the processing conditions. For example, if the material is strongly sheared during the process, dynamic yield stress should be used, mainly for flowable material. Otherwise, static yield stress is more appropriate.

Depending on the extrusion process chosen and the material properties, the final cross-section of a printed layer can take different shapes. Adapted from the work of Roussel [22], Mechtcherine *et al.* [9] and Carneau *et al.* [49], Figure 3 shows different cases occurring during deposition by extrusion of materials with different yield stresses and printing strategies. In cases a) and b), the deposited material is already flocculate, and its final shape is imposed by the nozzle cross section. For cases c) and d), the material is shaped and spread under self-weight or under the pressure applied by the printhead.

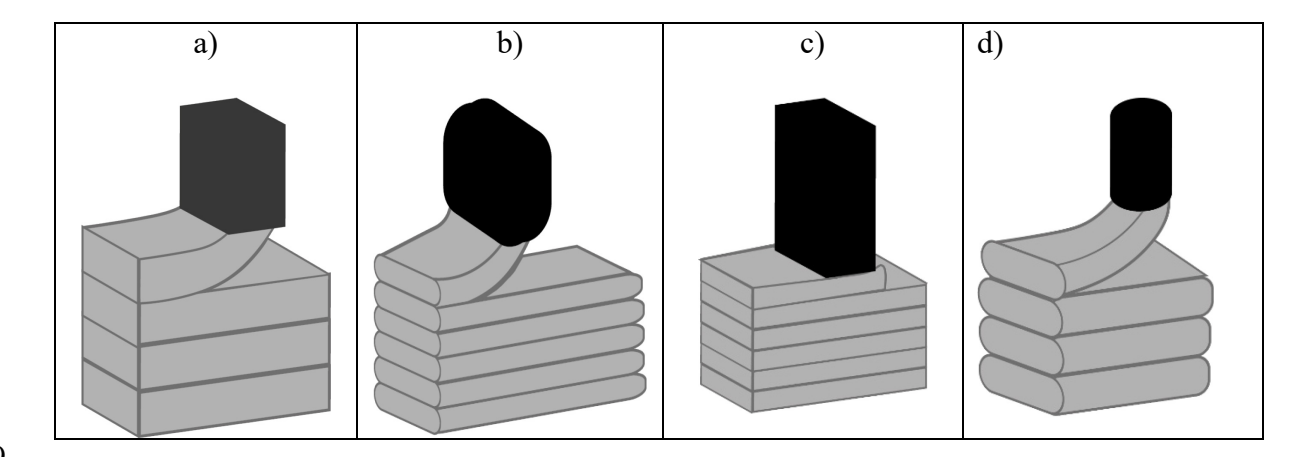


Figure 3: Different layer shapes obtained with existing printing strategies: a) Infinite brick; b)
Shaped brick by means of nozzle geometry reduction; c) material shaped under the pressure
applied by the printhead; d) flowable material spreading during deposition

In the case of the infinite brick, flow can be assumed to be elongational, and the material yield stress should fulfill at least the condition given by Eq. (9) to ensure the targeted layer height H_{layer} . Thus the targeted yield stress should be at least 12.5 Pa per millimeter of layer thickness (for a density of 2.2 g/cm³) [9]. This equation can be used independently of the shape of the cross section [50]. In the present form, eq. (9) considers the additional pressure applied by the nozzle during deposition, P_{nozzle} :

$$269 \qquad \frac{\rho g H_{layer} + P_{nozzle}}{\sqrt{3}} \le \tau_0 \tag{9}$$

Considering a highly flowable material, cases c and d, it can be assumed that if pure shear flow occurs the material will spread and the final thickness of the layer can be computed using the spread flow theory developed by Roussel and Coussot [9,51–53]. The sample height as a function of the distance *r* from the sample center can be obtained from the following equation:

274
$$H_{layer}(r) = \left(\frac{2\tau_0 \left(B_{layer} / 2 - r\right)}{\rho g}\right)^{1/2}$$
 (10)

- Where B_{layer} is the width of layer that can be computed from the equation of volume conservation. For highly flowable materials, surface tension effects could also contribute when $H_{layer} < \sqrt{\gamma/\rho g}$, i.e. layer thickness is lower than a couple of mm if we assume a surface tension effect of the cement similar to the surface tension of water [22]).
 - The shape of the deposited layer depends as well on kinematic considerations. The expected cross-section of the extruded filament is obtained if the extrusion flow rate Q_e is defined as $Q_e = V_r S_{nozzle}$, with V_r the printhead displacement velocity. Coordination between the robot displacement velocity and that of the material exiting should be achieved to avoid surface cracking, layer bending or even coiling [9]. If $Q_e < S_{nozzle} V_r$, under-extrusion, which generates tensile stresses, can occur, and if $Q_e > S_{nozzle} V_r$, over-extrusion, where compressive stresses occur during the deposit of the printed material. For example, a discrepancy of 10% between

- 286 the extrusion velocity and the velocity of the robot can induce deformation of 30% in the
- 287 materials deposited, which is sufficient to lead to material shear and fracture, and can initiate
- 288 the failure of the in-print structure. Description of the discrepancy between the real section of
- the layer and an ideal rectangular section can be expressed as:

$$\frac{\pi D_{nozzle}^{2}}{4\pi B_{laver}H_{laver}} = \beta \frac{V_{r}}{V_{e}}$$
(11)

- For the pressing strategies (cf. fig d)), a second kinematic condition depending on the extrusion
- speed V_e and the robot displacement velocity V_r can be expressed as:

$$293 H_{layer} = D_{nozzle} \frac{V_e}{V_r} (12)$$

- From results of Carneau et al. [49] it seems that an overall criterion defined as the ratio of the
- 295 pressing force F_{nozzle} and the stress induced by the self-weight of the material, defined as
- 296 $\frac{4F_{nozzle}\sqrt{3}}{\pi D_{nozzle}^2 \rho g H_{layer}}$ shows that decreasing H_{layer} below 1 cm allows having a pressing force which
- is greater than the self-weight of the material if Eq. (12) is fulfilled.

2.4 Structural behavior during 3D printing

- 299 It is now accepted that the absence of formwork in the extrusion-based 3D concrete printing process gives rise to the possibility of structural failure during 3D printing [22,54–58]. The 300 301 gradual increment of loading due to the self-weight of successive layers can lead to either *elastic* 302 buckling, instability failure, or plastic collapse, material yielding, of the unsupported printed 303 structure. To prevent the occurrence of these failure types, both the strength and the stiffness 304 properties of the freshly extruded concrete should develop sufficiently rapidly to keep up with 305 the increasing self-weight [59]. This increment of loading is likewise time-dependent and defined by the rising speed of the object, which in turn follows from the contour length of the 306 printed layer, the printing velocity, and the filament geometry. To assess whether structural 307 integrity is maintained during the printing process, various analytical methods have been 308 309 presented that relate the (minimal) development of material properties to the (maximal) rising 310 speed of the printed object.
- The development of the material strength of fresh concrete, or static yield stress τ_0 , is typically
- captured through the parameter A_{thix} [60], which is a measure of the structural build-up rate of
- fresh cementitious materials at rest (Eq. (13)).

314
$$au_0(t_{rest}) = au_{0.0} + A_{this} t_{rest}$$
 (13)

- Where t_{rest} is the time at rest after deposition and $\tau_{0,0}$ is the initial yield stress value. Depending
- on the time frame considered, the structuration rate may be described by both a linear and non-
- 317 linear trend [61–63]. Perrot et al. [64] presented a theoretical framework to define the optimal
- build-up rate in a 3D concrete printing process considering plastic collapse, given both linear
- and non-linear structural build-up of the yield stress. Basically, it permits estimation of a critical
- object height $H_{c,coll}$ which induces the plastic collapse of the first layer:

$$321 H_{c,coll} = \frac{\sqrt{3}\tau_0(t_{pr})}{\rho g} (14)$$

- Where t_{pr} is the time elapsed since the beginning of the printing. Wangler *et al.* follow a similar
- 323 approach to define the maximal horizontal printing velocity $V_{r,max}$, above which plastic collapse
- 324 would occur [65]:

325
$$V_{r,\text{max}} = \sqrt{3}L_{contour}A_{thix}/(\rho g H_{layer})$$
 (15)

- Where $L_{contour}$ is the contour length.
- 327 In addition to these plastic collapse criteria, Roussel [22] presented an analytical method to
- define the critical object height $H_{c,buck}$, at which elastic buckling is expected to occur:

$$329 H_{c,buck} = \left(\frac{8EI}{\rho gA}\right)^{1/3} (16)$$

- Where E is the elastic modulus of the material, I is the quadratic moment of inertia, and A is the
- horizontal rectangular cross-sectional area. Here, it should be noted that the requirement on the
- elastic Young's modulus to prevent buckling rises with the cube of the object height, whereas
- the yield stress requirements to prevent plastic collapse increases linearly with H.
- The elegance of these analytical methods lies with the ease with which they can be rewritten to
- define both the development of material properties as well as the allowable printing speed.
- 336 Instantaneously they can provide a first estimation of these requirements in preventing
- 337 structural failure during 3D printing. There is, however, a price to be paid for their simplicity.
- 338 These methods do not consider the gradient of material properties or variations of process
- parameters over object height and are independent of object geometry. Particularly in the case
- of elastic buckling, the geometrical contribution to the object's stiffness can be substantial, and
- thus, its omission in analytical methods can introduce a significant error. For these cases, where
- more accurate assessment is desired, the use of numerical modelling provides a solution.

2.5 Material drying and curing

- In extrusion-based 3D printing, fresh cement-based material is deposited without use of a mold.
- 345 Thus, it may dry significantly before setting. Drying decreases the amount of water available
- 346 for hydration. In the case of limited initial water content, water loss can be significant enough
- 347 to affect the hydration process. This problem is limited to millimeter-sized layers, where the
- 348 surface-to-volume ratio is high. Usually, bulk hydration is not affected by drying because the
- loss of mass is small compared to the total mass.
- However, the water loss may be localized at the free surface. Then, in a thin crust, hydration
- may not be complete, leading to weak mechanical properties of the interface between successive
- layers [66]. Keita et al. showed that the interfacial strength between two layers of mortar
- successively cast with a time gap of up to a two-hour interval depends on the initial water to
- cement ratio (W/C). For high W/C, the interface strength is as good as the bulk set material;
- whereas for W/C lower than 0.35, the strength is halved; see Figure 4. Moreover for weak
- samples, formation of a crust occurs [66].

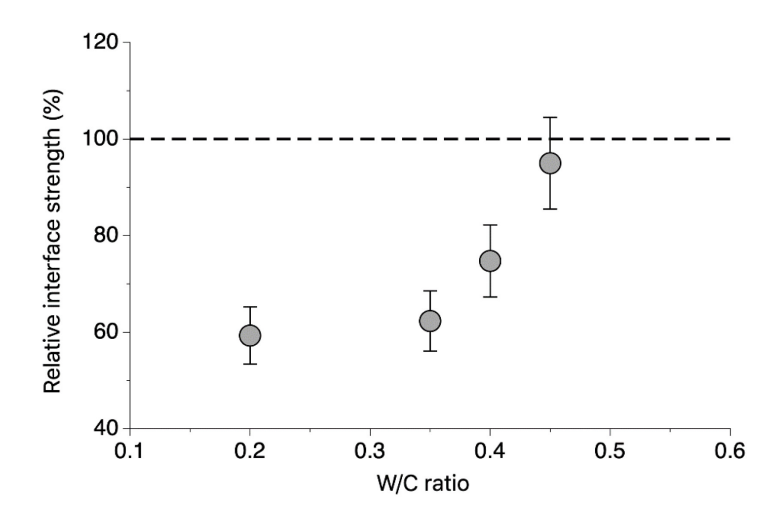


Figure 4: Relative interface strength as a function of W/C ratio after two-hour rest between mortar layers. Dashed line represents the reference level for bulk materials. Adapted from [66].

Dried crusts at the free surface occur due to the water flow inside the material to respond to the evaporative demand. As water evaporates, suction leads to liquid flow inside the porous structure [67–69]. If flow is fast enough, the evaporated water is compensated, water distribution remains homogenous, and the cement hydrates evenly. The maximum pressure drop is equal to capillary pressure and allows estimation of water flux J_{cap} inside the material. To avoid the formation of a crust and provide water to the surface, the following condition should be fulfilled:

$$367 J_{cap} > J_e (17)$$

368 where J_e the initial drying flux at the free surface.

In practical applications [68,70], the condition can be rewritten as $J_{cap} > 5 \cdot J_e$. The drying flux J_e at the free surface is:

$$J_e = -\frac{1}{\rho_w S_{air}} \frac{dm}{dt} \tag{18}$$

Where ρ_w is the water density, S the surface exposed to air, and m the sample mass. At room temperature and under laboratory conditions, the drying flux J_e , as defined in eq. (18), is around 10^{-7} m/s, corresponding to a water loss of 0.1 kg/m²/hour. However, the drying rate can vary significantly depending on external conditions such as temperature, humidity, and wind. For 3D printed cementitious materials, the temperature may be increased significantly over 20^{-25} °C, due to friction during extrusion and the use of accelerators. This may increase the drying rate by a factor of up to 100 above that of room temperature, leading to a value of J_e ranging between 10^{-8} and 10^{-5} m/s. Practically, the drying flux can be easily measured by the initial drying rate divided by the free surface of the sample. In case the material is not available for tests, the initial drying rate can be estimated by drying a cup filled with water.

The other member of equation (17), J_{cap} evaluates the flow capacity under capillary pressure P_{cap} , and can be estimated by the Darcy flow over the height of the printed element (*H*) [67]:

$$384 J_{cap} = \frac{\phi}{\mu + H} k P_{cap} (19)$$

- Where ϕ is porosity, μ_{water} fluid viscosity, and k permeability. The viscosity can be considered
- as that of water so long as few polymers are in solution. Indeed, unabsorbed polymers may
- increase the viscosity of the interstitial fluid between the cement grains by a factor of up to 100.
- Thus $\eta = 1 100$ mPa.s. The capillary pressure $P_{cap} = \gamma/r_p$, where γ is the air/liquid surface
- 389 tension. Surfactants could decrease the surface tension effect by a factor of 2; otherwise
- 390 air/water surface tension is 70 mN/m. The radius of the pore r_p in the cement paste depends on
- 391 the particle size distribution of the powder and its packing density. For classical cement with
- grains of approximately 10 μ m median size, the pore size r_p is around 1-2 μ m [71].
- 393 The permeability k of cement-based materials can be experimentally measured [72]. However,
- 394 the right order of magnitude of k can be estimated by the Kozeny-Carman formula k =
- $d^3r_p^2/45(1-\phi^2)$. The characteristic radius for liquid flow is considered to be of the same
- order as the radius for capillary pressure, i.e., around 1 μ m. The porosity ϕ depends on the
- mixture design, and can be calculated from the volume fraction of aggregates [73] and W/C
- leading to permeability values ranging from 10^{-15} to 10^{-16} m² for mortars.
- Finally, under laboratory conditions, J_{cap} varies from 0.01 times to 10 times J_e . To avoid drying
- 400 issues, eq. (17) should be fulfilled. Thus, in many circumstances J_e should be decreased or J_{cap}
- 401 increased. As J_e depends mostly on external conditions, decreasing the water demands
- 402 correspond to decreasing the temperature and the wind velocity, or increasing the humidity.
- 403 J_{can} depends mostly on W/C and the aggregate volume fraction: from W/C = 0.45 to 0.2, J_{can}
- decreases by a factor 10. Indeed, such variation is high enough to yield heterogenous mortar
- and a weak interface, as shown in Figure 4, and increases the difficulty in 3D-printing concrete
- 406 directly onsite.
- In addition to interface layer weakness, shrinkage can be detrimental to a 3D printed structure.
- 408 It occurs under dimensional instabilities because of the movement of water molecules or
- 409 volume change of reaction products in general. Typically total shrinkage $(\varepsilon_{total}^{sh})$ can be
- represented as the sum of plastic (ε_p) , drying (ε_d) , autogenous (ε_{auto}) , and carbonation (ε_c)
- 411 shrinkages [74,75] as shown below:

412
$$\varepsilon_{total}^{sh} = \varepsilon_p + \varepsilon_d + \varepsilon_{auto} + \varepsilon_c$$
 (20)

- The total long term shrinkage strain in concrete is primarily effected by drying shrinkage;
- 414 autogenous shrinkage contributes only 5% of the total strain, and carbonation is more of a
- surface effect [76]. However, plastic shrinkage can be detrimental to 3D printed structures in
- 416 the short-term especially because of the unique rheology of the mixtures and the higher surface
- 417 area-to-volume ratio, which could cause cracking, roundness errors, or even structural collapse
- 418 [77].
- There are different models and equations to account for and predict shrinkage in concrete and
- similar cementitious systems. The most common ones include the ACI 209-82 model [78,79],
- 421 CEB-FIP model [80], and B3 model [80–82]. Generally, shrinkage is associated with the drying
- of the surface as a result of evaporation and bleeding, which increase pore pressure and the
- 423 radius menisci which induces stresses in the pore. Figure 5a shows the variation of capillary
- pressure when evaporation overtakes bleeding and there is a net loss of water from the surface

of a cast concrete specimen. Figure 5b shows the mass loss over time where the initial bleeding compensates for the evaporation loss. But beyond the intersection point of the graphs, drying induces shrinkage. There have been several models developed to quantify and simulate the shrinkage process. The most common and fundamental model is of the form [83] as:

$$\varepsilon_{sh} = \alpha_{sh} H_{\%} \tag{21}$$

where α_{sh} is the coefficient of shrinkage and $H_{\%}$ is the ambient relative humidity. Other models consider shrinkage strain based on capillary pressure [84], partial saturation levels in porous solids [85], simultaneous action of capillary pressure and disjoining pressure [86], water content [87,88], and moisture diffusion [89,90]. Several works have developed models in terms of a severity index [91] and plastic shrinkage cracking [92], both of which are specifically applicable to immediate plastic shrinkage which is relevant in the fresh conditions of cement mixtures in the immediate printed state. The main differences that conventional models for cast in-situ concrete differ from printed elements in shrinkage is the need to model the effects of differences in the fundamental mechanisms inducing the shrinkage process. The main differences include a) the primary significance of plastic shrinkage, b) the combined effect of the squeezing of layers along with capillary bleeding-induced evaporation, and c) the direction of water loss through multiple exposed surfaces when compared to the vertical-only direction in the case of a closed mold casting.

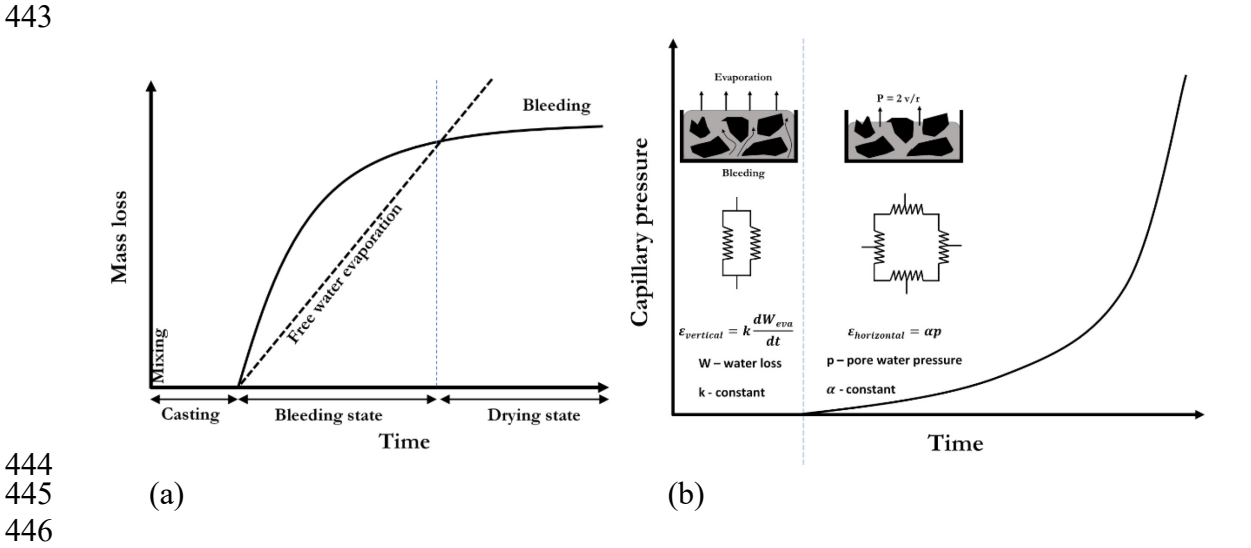


Figure 5: Shrinkage modelling for 3D printing of cement concrete (3DPC) - (a) pressure evolution with time [93] - (b) Bleeding vs. drying state [94]

The exact description of the heterogeneous nature of shrinkage in a complex 3D printing process requires the development of dedicated numerical simulation tools which consider complex shapes and pertinent boundary conditions.

3. Toward a numerical toolbox of methods for the 3D printing process

3.1 Mixing step

Analytical methods to assess mixing procedure require an experimental campaign to evaluate the concrete's homogeneity. However, such experimental work needs expensive tools because concrete is opaque and visual inspection remains insufficient for assessing concrete quality. Even though it is possible to model the flow in a truck mixer geometry using the finite volume

method (FVM) using a supercomputer as shown in Wallevik and Wallevik [95], the preferred methods to study the mixing step using numerical tools is based on DEM, distinct or discrete elements methods [96,97].

This method, originally developed to study the dynamics of granular media [98], was implemented to study concrete flow in the 1990s [99,100]. It considered cementitious material as a network of separate particles interacting with each other. Forces among the particles are computed using relevant interaction laws. Newton's second law allows the computation of the displacement of each particle considering the forces due to its interaction with surrounding particles during a fixed time step. This time-iterative procedure is repeated in order to obtain the description of the flow of concrete during the entire period under study.

To describe the flow of cementitious materials accurately, it is crucial to use relevant force-displacement relationships. Both so called "contact laws" are needed for the normal and tangential direction to the particles' surfaces in order to describe the global viscoplastic behavior as expected of the flow of fresh cementitious material. For example, as proposed by Mechtcherine *et al.* [96,101], a combination of dashpot, springs and sliders provides a physically acceptable force-displacement relationship between aggregates embedded in a cement paste, as shown in Figure 6.

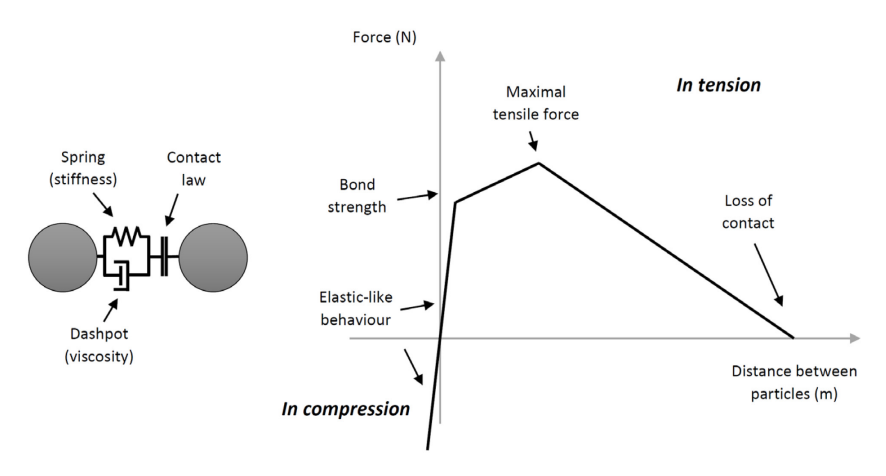


Figure 6: Example of a force-displacement relation in the normal direction used to model the interaction between two aggregates embedded in a cement paste or a mortar (adapted from [101]).

DEM has been applied to the mixing of cementitious materials because it allows for the fast visualization of the quality of the mixing process by using particles of different colorations, initially separated [96,102]. Moreover, DEM can also be used to study the segregation and dispersion of particles having different sizes, i.e. sand and gravel.

More recently, progress in computation methods has facilitated the development of more complex contacts laws, using time-dependent contacts laws [103] or also for different types of particles, e.g., liquid and solid particles. It leads to the fact of different types of force-displacement relationships being useful within the same time-step of a numerical simulation, depending on which types of particles are in contact [104].

For example, Krenzer *et al.* [104] modelled the mixing of cementitious materials, taking into account the transfer of water content during the interaction of a solid dry particles with a liquid droplet. Such numerical simulation of the mixing requires the use of evolving contact laws that

- describe the transition of dry bulk material to a suspension depending on the local water content.
- This type of numerical simulation paves the way to the numerical study of the dispersion of
- accelerator within the printhead. The use of DEM for this purpose is expectantly awaited in
- order to optimize nozzle shapes and in-line mixing systems.

3.2 Material delivery

497 3.2.1 Pumping

- 498 Similar to analytical tools, there have been many numerical tools developed for simulating
- 499 concrete pumping process. So far, the numerical tools have been focused on enabling estimation
- of pumping pressures in consideration of the concrete's rheological properties, influence of the
- 501 lubricating layer and its properties, and process pipeline variations, including bends and
- diameter changes. The following is a brief summary of selected numerical modelling works on
- 503 the concrete pumping.
- The majority of the published research on numerical modelling of concrete pumping utilizes
- 505 the Computational Fluid Dynamics (CFD) approach [17,97], in which concrete is modelled as
- one single or as multiple phases in a continuum. This means that the rheological properties of
- 507 concrete in a phase are constant throughout the modelled geometry. A numerical solution for
- fresh concrete's rheological behavior is then made possible using the conservation laws or the
- Navier–Stokes equations in conjunction with the Bingham or Herschel-Bulkley models.
- Jo et al. [17] developed a computational approach to estimate the lubricating layer (LL) in
- 511 concrete pumping. Choi et al. [105] simulated fresh concrete flow in a 170 m long pumping
- 512 circuit using a single-fluid CFD approach. The best fitting thickness for LL was determined by
- 513 comparing calculated pressure with the experimentally measured values at a flow rate of 50
- 514 m^3/h . Furthermore, they analyzed pressure profiles comparatively along the circuit geometry
- with the pressure profiles measured experimentally [105]. Choi et al. [106] investigated the
- 516 formation of the lubricating layer and simulated the mechanism of shear-induced particle
- 517 migration (SIPM) during concrete pumping. Influences of particle shapes were indirectly
- modelled by solving SIPM equations, and by implementing a User-Defined Scalar into ANSYS
- Fluent [106]. It was found that numerical simulations considering particle shape correlated well
- with experimentally measured velocity profiles using an Ultrasonic Velocity Profiler. Chen et
- 521 al. [107] performed CFD simulations of wet shotcrete flow in a pipe and determined the
- 522 thickness of LL. Tan et al. [108] developed a multi-phase numerical model to investigate wear
- mechanisms of a concrete piping wall. They combined DEM and CFD approaches: DEM to
- model concrete aggregates as discrete particles and CFD to model the continuous fluid phase.
- Nerella et al.[109] developed a single-phase CFD model for simulating SLIPER experiments,
- 526 in which the lubricating layer was implemented using a user-defined function to vary the
- material properties radially, as in experiments. Secrieru *et al.*[21] implemented similar model
- 528 in large-scale pumping simulations of various types of concretes. If the rheological properties
- of the LL cannot be experimentally determined, then they can be estimated indirectly using
- numerical simulations in combination with analytical particle-suspension models such as
- Chateau-Ovarlez-Trung and Krieger-Dougherty models, as shown by Nerella *et al.*[109].
- All these abovementioned tools could be applicable for 3D-printable concretes. However, there
- are certain research challenges that still need to be addressed:
- Pumping during printing is often interrupted to move the printhead to new printing position or to leave a wall opening, e.g. for windows, etc. As reported in the

- experimental work of De Schutter *et al.*[110], pumping pressures after a break could increase drastically. Implementation of thixotropic material models is therefore of high significance to develop numerical models as comprehensive tools in simulating the pumping process of printable concretes. De Schryver *et al.*[111] validated implantation of thixotropy in CFD by linking the thixotropic internal structure to concrete viscosity.
- Experimental investigation focusing on the pumping of high-yield-stress, printable concrete with various degrees of thixotropy are yet to be reported and are needed to be conducted in conjunction with verification of analytical and numerical tools.

545 3.2.2 Extrusion

536

537538

539

540541

542543

- 546 The use of numerical methods in studying the extrusion of cementitious materials allows the
- description of the occurrence of multiphase flow and to account for the heterogeneous and
- 548 multi-scale nature of cementitious materials.
- For example, El Cheickh et al. have modeled the extrusion flow of cementitious materials using
- 550 DEM [44]. The authors have used so-called soft-shell contact [112] considering each particle
- as a composite material consisting of a hard core, the aggregate, surrounded by a soft shell, the
- suspending cement paste. Using this method, the authors were able to determine the maximum
- diameter of sand particles and sand volume fraction that can be used in a mortar mix-design of
- a specified cement-paste rheological behavior. Where more complex geometries are involved,
- e.g., a section-varying screw extruder [113], it can be noted that DEM has also been used to
- simulate the orifice extrusion of cementitious materials or to predict the flow-induced
- orientation of fibers within an extruded layer [96,114].
- With the ability to model individual constituents discretely with sizes of a few millimeters and
- actively track their particle level interactions, DEM simulations offer efficient tools for
- extrusion processes. Recently the researchers of IAB Weimar GmbH and TU Dresden,
- collaboratively developed a DEM simulation model of a large-scale screw extruder that can
- extrude concretes with aggregates up to 8 mm diameter. Results showed that DEM can be
- 563 utilized to model material flow of heterogeneous high-yield stress printable concretes in
- complex extruder geometries accurately; see Figure 7.

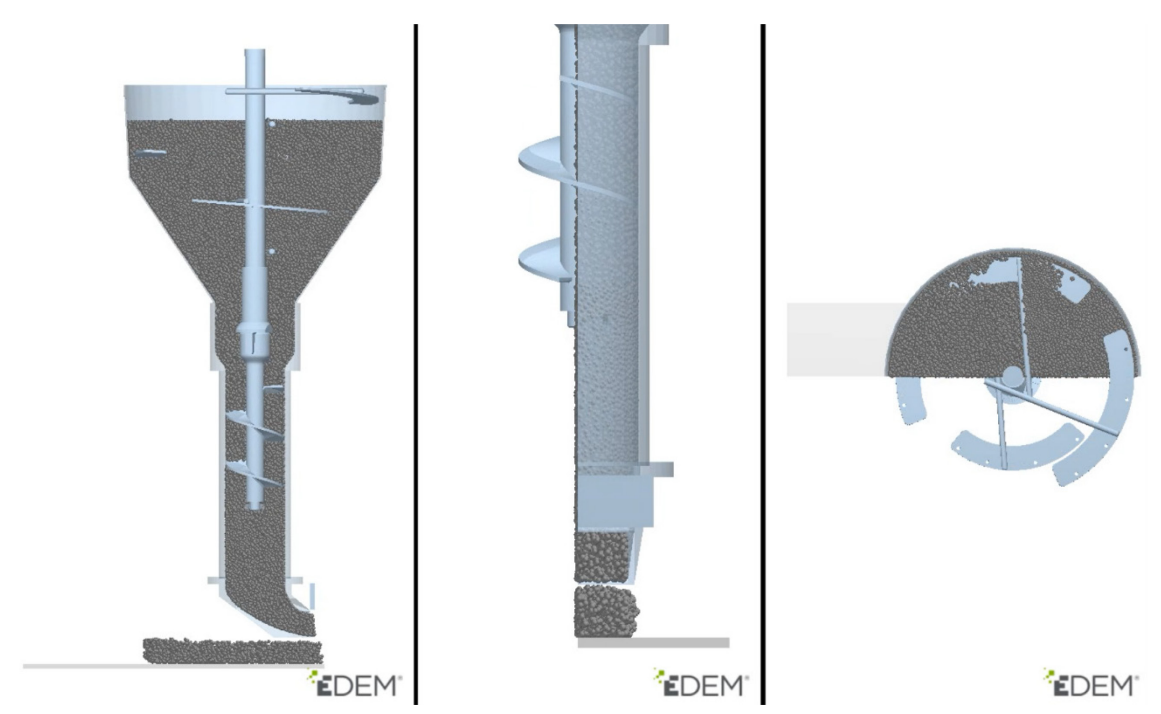


Figure 7: Simulation of printable concrete in large-scale screw extruder elucidating both extrusion and deposition processes (Courtesy of: Knut Krenzer, IAB Weimar gGmbH).

It is also important to note that water drainage during extrusion has been modeled using a finite difference method [115]. Using an adapted version of the Terzaghi consolidation theory, this model allows the practitioner to describe the local evolution of the water content and the rheological behavior of cementitious materials undergoing extrusion. In the framework of this study, the authors also developed a description of the mechanical behavior with a transition from visco-plastic to pressure-dependent Coulomb type frictional material. This method can be helpful in order to ensure that the material remains homogeneous during extrusion, where consolidation kinetics are far slower than the process kinetics, and merits being extended to two- or three-dimensional problems.

3.3 Material deposition

- The use of numerical simulation based on finite element methods for the deposition step during cementitious materials 3D printing is very useful in order to obtain the exact shape of the deposited layer in real cases that are between asymptotic cases presented in section 2.3. Moreover, it allows estimating the stress distribution within the layer to predict crack formation or surface defects.
- Several options exist for modeling the flow behavior of mortars and concretes during the material deposition step: an elastic-visco-plastic model [51], a bi-viscous model where two viscosities are used to simulate rheological behavior up until and the subsequent to exceeding the yield stress of fluids [116] [117] or a continuous visco-plastic model [118,119]. For the elastic-visco-plastic model, the material follows a Kelvin-Voigt model up to the yield stress and behaves as a Bingham fluid beyond the yield stress. This approach consists in adding a high enough Young's modulus such that the material's elastic deformation remains negligible in comparison with viscous deformation.
- The robustness of the numerical modelling of deposition also depends on achieving repeatable rheological measurements before prototyping the final component, as presented in [120] and [22]. To include reliable material properties, especially for high yield-stress materials, viscosity

evaluation may not be easily evaluated [121]. Experiments inspired by soil mechanics or hardened concrete testing can be used, for example, to estimate the elastic properties of the material [54,122].

The sketch of a numerical simulation of mortars or concretes extrusion can be found in [123]. The Finite Volume Method (FVM) [123–125], using CFD (Computational Fluid Dynamics) or PFEM (Particles Finite Element Method) [126] [127] can be used to simulate printed layers using a complex fluid assumption. Such methods use a Lagrangian framework with an updating mesh. The PFEM approximates the behavior of the material using a Perzyna formulation, a rate-independent yield function used to describe the visco-plastic strain, of the Bingham model that allows the taking of elastic deformation before material flow into account.

Using FVM it has been recently shown [128] that if robotic arm velocity suits the material flow rate, nominal speed, and nozzle cross-section, then no variation in stress distribution occurs in the filament. Such numerical modelling highlights the notion that increasing deposition height or material properties such as stiffness, yield stress, and viscosity can be used to avoid overextrusion or even buckling of the filament [128]. Also, if under-extrusion occurs, then a reduction of the maximal strain that the material can withstand before yielding reduces the tearing of the filament [128].

The PFEM, in which a system of equations is solved by a set of pseudo-particles, which are discretized by standard finite elements, is used in [127] to simulate the extrusion process and predict layer shape. Figure 8 shows simulations of the influence of material flow rate on layer cross section. Reinold et al.[127] reported that with PFEM, computed and measured cross sections differ by less than 1% if the scaling of the velocity, nozzle section, and flow rate process parameter is carried out. Extrusion-induced dynamic forces act on the top of the currently printed wall segment and may influence the early age stability of the structure. As proposed by [127], a generalized conclusion on the optimal tuning of the material properties is not yet possible based on numerical results only.

(a)

591

592

593

594

595

596

597 598

599

600

601

602

603 604

605

606

607

608

609

610

611 612

613

614

615 616

617





(b) Height [cm] $Q=1.0\cdot Q_0$ $Q=1.2\cdot Q_0$ -3 0 3 Width [cm] (c)

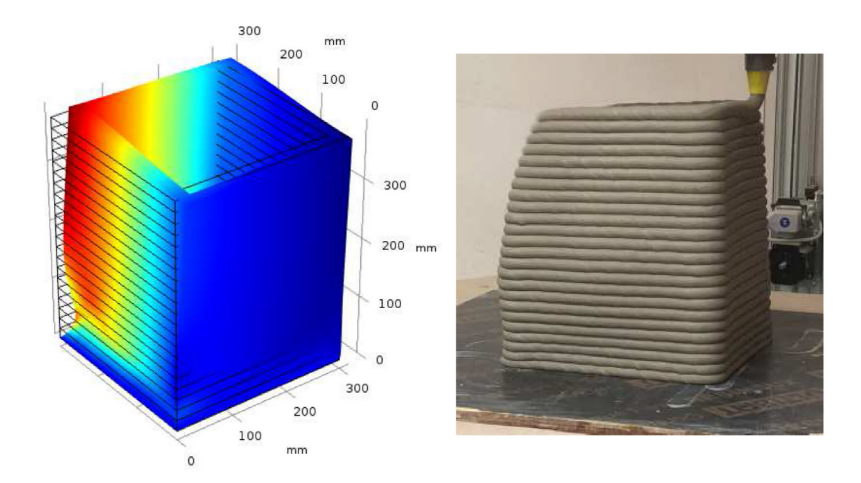
Figure 8: a) Experimental result with constant flow rate (right wall), b and c) PFEM numerical simulation of geometry variation with varying material flow rate, here $Q_0=0.0001053~\text{m}^3/\text{s}$. (Courtesy of Janis Reinold, Ruhr-Universität Bochum).

Concerning useful improvements that need to be implemented in the numerical modeling of the deposition phase, elastic-visco plastic models could provide new insight by modeling creep flow which cementitious material can undergo. Moreover, thermo-mechanical modelling should be included, as in the case of the infinite brick process, friction can lead to a temperature increase within the material and thus to a different stress distribution as well as for flowable material where accelerators are added just before deposition, thereby very rapidly increasing the temperature of the material. Also, physical properties such as the porosity induced by the process can be optimized by modeling the meso-structure.

The time required to carry out complex numerical modelling is relatively long and needs to be reduced. Assuming symmetry or axisymmetric conditions can also reduce computational cost. Optimization loops used to fit the input parameters of numerical modeling should be carried out to improve the deposit modeling; digital image correlation or calorimetry tests can be used, for example, as non-destructive tests to assess the reliability of the numerical model used. This has begun to be done in the work of [129], in which the model input parameters are initially determined and then subsequently adjusted through an optimization loop minimizing the difference in the displacements predicted by the model and the measurements which could be performed by ultrasound examination or digital image correlation.

3.4 Structural behavior during 3D printing

The maturity of 3D concrete printing is reflected by the increasing complexity of objects created by the technology. Bespoken architectural elements and objects with optimized material usage are appearing in practice, and the potential of on-demand or graded material printing strategies is being explored. For such advanced geometrical features and material distribution, the application domain of analytical methods is quickly exceeded. Moreover, while the main loading condition during 3D printing may be the self-weight of printed objects, as object complexity increases, other loading types may occur due to the eccentric placement of layers, kinematic pressure in the deposition process [49], or non-vertical pressure by secondary materials [9,54]. In this regime, numerical modelling can provide detailed insight into structural behavior as well as the occurrence and type of in-print failure as demonstrated by Figure 9 that shows the comparison between the printing of an empty column of mortar and its numerical simulations. In this 3D Finite Element Method (FEM) model, the material is modelled using an elasto-plastic behavior using a pressure-dependent plastic criterion (Coulomb's law).



651 Figure 9: Compar

Figure 9: Comparison of printing process with numerical simulations. Description of shape-dependent complex failure model. Color-scale provides the level of displacement (Courtesy of R. Hameed).

The application of numerical methods in controlling structural behavior during 3D concrete printing was for the first time demonstrated by Wolfs *et al.* [54]. A 3D FEM model has been developed, which simulates the successive placement of filaments during the printing process and the corresponding development of material properties and self-weight loading. By linking the FEM model to 3D CAD software, and including process parameters such as the printing speed, the numerical model is essentially a digital twin of the 3D printing process, and thus, can theoretically consider any complex geometry, variation in material properties, as well as loading and support conditions. As the model includes both strength and stiffness parameters, and features a geometrically non-linear analysis, the structural behavior during 3D printing can be studied systematically, considering both failure types of elastic buckling and plastic collapse.

Rapidly to evaluate whether a 3D printed wall structure is susceptible to structural failure during printing, Suiker developed a parametric mechanistic model [55]. The wide ranges of process parameters and material properties were in this model reduced to five unique dimensionless parameters to define both elastic buckling and plastic collapse. Suiker adopted a numerical procedure to formulate convenient design formulas and design graphs for the three geometrical cases of a free wall, a simply supported wall, and a fully clamped wall.

In a subsequent study [130], the two numerical approaches, an FEM-based and a parametric mechanistic approach, were compared. The input for these analyses was based on extensive experimental studies of the early age mechanical behavior of 3D printed concrete [122,131]. The numerical results of both methods were found to be in very good agreement. More recently a comprehensive experimental validation study was performed, demonstrating the transition behavior from elastic buckling to plastic collapse, the influence of geometrical imperfections on buckling failure, and the effect of printing speed (analogous to variations in structuration rate) on object stability. The results of these printing trials were in very good agreement with the numerical predictions, highlighting the potential of numerical methods in analyzing the structural behavior during 3D printing. Consequently, numerical methods may be adopted to define, for instance, optimal printing speed or the minimal structuration rate without the occurrence of failure during the 3D printing process. It is interesting to note that other research groups have started to develop FEM-based numerical simulations in order to study the structural behavior of in-print structures [129,132–137]. These studies are based on the same principles but use different criteria for plasticity and the modelling of the evolution of mechanical

- properties over time. Recently, Chang et al. developed an extended lattice model using a 3D
- network of Timoshenko beams with properties calibrated using green strength measurement of
- the cementitious materials in order to study the stability of the structure during printing [138].
- To model the process, the authors gave a gradient of mechanical properties to the beams along
- the structure height.
- While numerical methods are deemed more accurate than their analytical counterparts, the price
- to be paid is in computational cost. Particularly if both geometrical non-linearity for buckling
- and material non-linearity for plasticity are to be considered, and a complex 3D geometry is
- analyzed such that symmetry conditions cannot be applied to reduce model size, computational
- time can be excessive. This raises the question of accuracy versus speed and, more particularly,
- 695 the stage in which the assessment of structural integrity is to be performed. If an a priori
- assessment of the optimal printing speed or structuration rate is to be defined, dedicated FEM
- simulations may be a suitable strategy. However, as the 3DCP community is increasingly
- 698 moving towards real-time feedback and control as well as set-on demand strategies
- o98 moving towards real-time reedback and control as well as set-on demand strategies
- 699 [59,139,140], rapid decision making is required and to this end, a more simplified yet
- instantaneous analytical assessment may suffice.
- 701 Until now, material behavior is expressed exclusively as a function of time. However, it has
- been shown that additional environmental and process parameters can play a significant role,
- such as temperature variation during printing sessions, which has a significant effect on early-
- age strength and stiffness properties and, thus, on the occurrence of in-print failure [122,130].
- Also, the bond strength between filaments is a critical feature which has been shown to be in
- similar fashion strongly dependent on process parameters and environmental conditions
- 707 [66,141–143]. The inclusion of thermal and hygric parameters in the numerical simulations
- may serve as a first step in extending the simulation into the hardened phase, as shown in the
- 709 next part.

3.5 Material curing and drying

- 711 Specific numerical tools on drying and early shrinkage of 3D printed materials are still under
- development. Understanding the fundamentals of the shrinkage in printable mixtures helps in
- 713 modelling the phenomenon and applying it specifically to 3D printed (3DP) structures. Existing
- models on shrinkage in cementitious systems have to be coupled with structural and procedure-
- specific mechanisms in 3D printing for different materials such as metals, ceramics, polymers,
- etc. which can be used to model the shrinkage phenomenon in 3DP of concrete (3DPC).
- 717 Figure 10 shows the effects of differences in boundary conditions while modeling the moisture
- 718 loss that induces shrinkage of specimens in cast in-situ and printed specimens. Due to the closed
- boundaries, which do not allow any evaporation, the net evaporative flux is unidirectional, as
- shown in Figure 10a, under capillary action in cast specimens. However, additional squeezing
- under the overburden pressure of the layers and the open surfaces in the vertical direction need
- 722 to be incorporated for printed specimens.

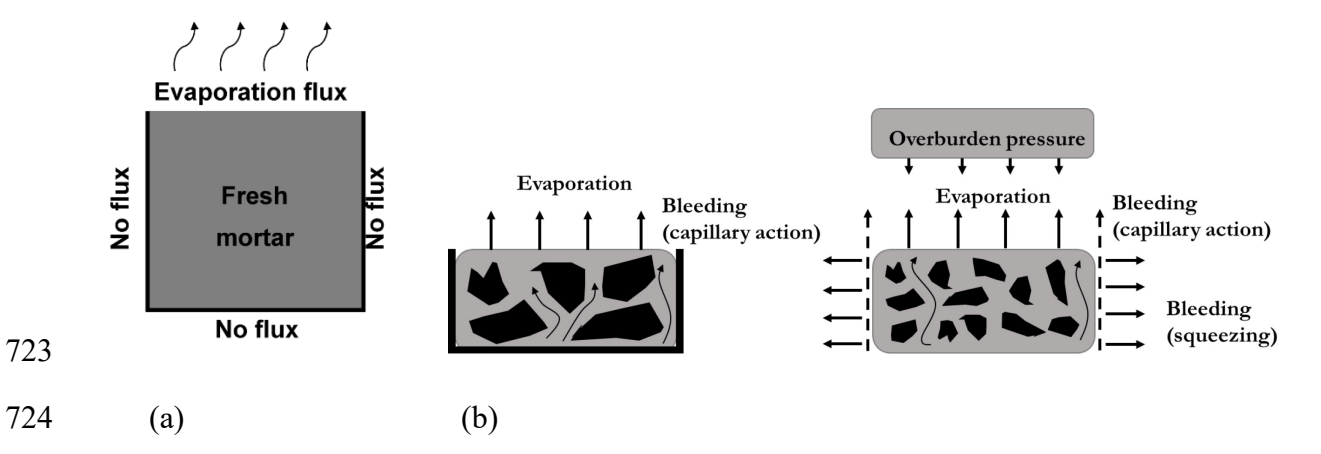


Figure 10: Difference in shrinkage modeling boundary conditions of cast in-situ and printed specimens. (a) Unidirectional evaporative flux in cast specimens [131]—(b) Cast in-situ vs. printed specimen boundary conditions in moisture loss

Modeling 3D printed systems for shrinkage is additionally challenging, considering the layered state of the system, which generally negates that innate assumption of isotropy and homogeneity of material characteristics. Figure 11a shows the staircase phenomenon in binder jetting [145] where layers differentially shrink at the boundaries and cause a trapezoidal edge. The time taken for each layer to be placed and the material structure evolution will be additional parameters that can address this effect in the case of cementitious binders. This idea can then be translated to appropriate model elements, e.g., Maxwell, Kelvin-Voigt, Burgers etc., to identify layer effects and appropriately address possible differential shrinkage as shown in Figure 11b [146]. Additionally, a 3D-lattice model to couple moisture diffusion and cracking in shrinkage for strain hardening cementitious composites [83] and discrete element models [147,148] are also proposed as suitable candidates to model these systems.

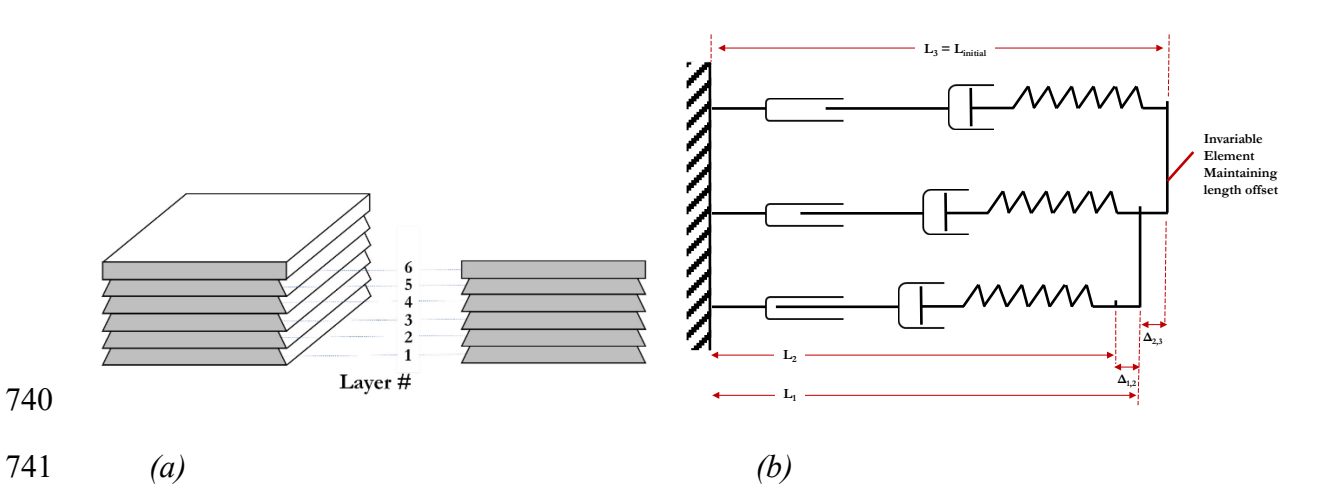


Figure 11: Different model provisions associated with 3D printed specimens - (a) Staircase effect in shrinkage of layered systems [145] - (b) Modelling elements for differential shrinkage in layered systems [146]

Although drying shrinkage in printable cementitious binders have been recently reported [149–151], the results were independent of the printing procedure and focused on material characteristics like the amount of nanopores, dispersion, specific surface area, and energy activity of solid phases [149]. The ACI and FIB models were used to evaluate drying shrinkage

in fiber-reinforced 3DP binders to propose a porosity based model in [150] while a novel

shrinkage measurement technique was proposed for 3D printed cementitious filaments in [151].

Due to the lack of literature in shrinkage model development in 3DPC, results from other fields

and materials could be relevant benchmarks for review.

It is relevant to note that in 3D printed Polylactic Acid (PLA) parts, the shrinkage decreases with an increase in layer height and print speed while it increases with print length [152], which could be relevant in the case of cementitious mixtures as well. Also, in metal fused filament fabrication (FFF), shrinkage is reported to be independent of the infill percentage [153] while fused deposition modeling (FDM) of PLA parts using viscoelastic models and numerical modeling have been used to develop interior structures (infills) that compensate for the overall shrinkage of the otherwise solid print. This information could be used to modify the model and print parameters in compensation modeling [153–157] for shrinkage mitigation. This shows that relevance of infill patterns to influence the shrinkage properties of printed structures. Hence, these remain as gaps in research and underly the significance of research in understanding the fundamental mechanisms and modelling approaches for plastic and drying shrinkage in 3D printed cementitious systems.

4. Summary and discussion of the relevant tools

Analytical models are useful in providing rapid insights into the rheological requirements and process parameters for 3D printing, but they are insufficient in real practice, i.e., with complex geometrical configurations, or when materials exhibiting gradients of consistency between self-consolidating materials and zero-slump concrete are used. For example, the analytical stability criteria proposed in Eqs. (14) and (16) enable prediction of the failure of the structure in the simplest case, i.e., with a constant rate of printing, perfectly vertical structures and also for Eq. (16) a material with homogeneous properties, but cannot be used to predict failure in real situations accurately. In these cases, numerical modelling methods are suitable to obtain precise prediction of the process. This practice paves the way to the in-line monitoring of the process through a digital process twin which can be used for process control, process calibration or material optimization.

However, if these tools exist, they must be optimized in terms of computation requirements and have their use simplified in order to be democratized on the industrial engineering scale. All selected methods detailed in this work are summarized in table 1.

Table 1: Summary of selected analytical models and numerical tools for each step of the printing process of cementitious materials.

Step	Equations / Tools	Model parameters			Ref
		Material	Process	Geometry	Rei
Mixing	Characteristic diffusion time - Eq. (1)	μ: viscosity r _{acc} : accelerator molecule radius			[9]
	Mixing kinetic law - Eq. (2)	t _c : characteristic mixing time	Ω: Mixing rate		[14]
	Numerical tools:				
	DEM methods with evolving and heterogeneous contact laws				[104]
Pumping		τ ₀ : shear yield stress μ: viscosity			[18]

	Kaplan flow rate predictions - Eq. (4) and (5) Numerical tools: Computational Fluid Dynami constitutive law CFD consideration of shear-indu	το,: wall shear yield stress μ.: viscosity inside the LL cs (CFD) approach to a control of the	Q_p : Pumping flow rate	length	[15] [17] [105] [106, 107]
Extrusion	CFD with heterogeneous materi Benbow-Bridgwater equation Eq. (6) Basterfield model Eq. (7)	als σ ₀ : yield stress (elongational) a ₀ , a ₁ , n ₀ , m: viscous fitting parameters τ ₀ : shear yield stress η, n: parameters of HB model (viscosity) τ _{0,i} : interface yield stress μ _i : viscosity inside the LL	V_{ext} : extrusion velocity P_{ext} : extrusion pressure	d_{die} : die diameter D_{ext} : extr. diameter L_{die} : die length θ : convergent flow angle	[29]
	Progressive cavity pump (PCP) flow rate Eq. (8)		Q_{pcp} : PCP flow rate n_r : rotational rotor velocity	e: excentricity V_{pcp} : PCP volume D_r : rotor diameter D_{st} ; stator diameter P_{st} : stator pitch	[41]
	Numerical tools: DEM with soft-shell contact law DEM with "Bingham" type interaction Layer height prediction:				
Deposit	Infinite brick asymptotic case Eq. (9) Layer height prediction: Free flow asymptotic case Eq. (10) Shape accuracy: Eq. (11)	ρ: material density τ ₀ : shear yield stress	P_{nozzle} : pressure exerted by the nozzle on the layer F_{nozzle} : force exerted by the nozzle on the layer V_e : extruded layer velocity V_r : Robot head velocity	H_{layer} : single layer height B_{layer} : single layer width β : geometrical accuracy parameter D_{nozzle} : Nozzle diameter	[9,22, 49] [9,53] [49]
	Numerical tools: Particles finite element method (PFEM) Finite volume method (FVM)				
Stability	Base layer plastic collapse: Eq. (14) (15) Elastic buckling failure: Eq. (16)	τ_0 : shear yield stress A_{thix} : structural build- up rate ρ : material density E : elastic modulus	V _{r,max} : Maximum robot velocity value for plastic collapse criterion t _{rest} : time elapsed since material is left at rest after deposit t _{pr} : time elapsed since print starts	H: height of the printed structure $H_{c,coll}$: critical height for plastic collapse $H_{c,buck}$: critical height for elastic buckling $L_{contour}$: contour length I: quadratic moment of inertia	[64]

				of the horizontal cross-sectional area A: cross sectional horizontal area	
	Numerical tools: FEM with elasto-plastic behavior with pressure dependent criterion Parametric mechanistic modeling Extended lattice network of Timoshenko beams with varying properties				
Drying and curing	Comparison between capillary and evaporation flux J_{cap} and J_e Eq. (17) (18) (19)	ρ_w : water density η_w : water viscosity k : permeability ϕ : porosity γ : air/water surface tension r_p : pore radius	J_{cap} : water flux induced by capillary pressure J_e : water evaporation flux	m: material mass Sair: free surface H: sample height	[66]
	Shrinkage Eq. (20) Numerical tools: Methods to be developed by imp geometry.	elementing cementitious	materials behavior	within 3D printing	[74]

5. Conclusions

This paper provides a review of the tools that can be used to describe the extrusion-based, 3D printing process of cementitious materials. A comprehensive review of the literature and a synthesis of all available models and tools are provided in the expectation of helping both academia and industry by making available an exhaustive toolbox that can be used at different stages of the development of a printing process, or for process monitoring. The paper follows the process from the initial mixing to the early curing conditions which can alter the final hardened behavior of the printed concrete.

In the first section, analytical models that can be used to provide approximate estimations of rheological requirements of the materials and/or the process parameters are enumerated. Kinetics of mixing, equations linking flow rate and pumping/extrusion pressure, prediction of the layer height of fluid and firm cementitious materials (i.e. asymptotic cases), stability criterion for in-print structures with simple geometry and description of adequate curing conditions are presented. It is shown that these methods can be used for simple cases or as a first estimation attempt in the early development of a new process by considering simple asymptotic cases, i.e., infinite brick or highly flowable material.

However, it is also shown that the above methods are not accurate enough to provide a complete and comprehensive description of the process. It makes them inefficient in optimizing the 3D printing process or for in-line monitoring. For this purpose, advanced numerical solutions have been or are being developed. These numerical approaches are listed in the second section.

It has been shown that DEM, the Distinct Elements Method, is very promising for the simulation of the mixing process, initial or in-line, and for the prediction of granular blocking during extrusion and pumping. Moreover, FEM, the Finite Elements Method, is able to simulate the deposition step and provide the description of the shape of the deposited layer or to predict the stability of the structure during printing. These advanced numerical tools can be used for optimizing the printing process in the case of the printing of complex shapes and can be used with appropriate complex constitutive laws such as time-dependent behavior, pressure-

- 813 dependent behavior, thermal and hygric effects etc., and for gradients of properties and
- 814 composition.
- All the methods are listed in a final table, which can serve as a toolbox reference for engineers
- developing printing processes or building increasingly complex printed concrete structures.

817 References

- 818 [1] J. Maier, Made Smarter Review, Department for Business, Energy and Industrial Strategy: 819 London. (2017) 230.
- 820 [2] HM Government, Industrial Strategy: building a Britain fit for the future, (2017). 821 https://www.gov.uk/government/publications/industrial-strategy-building-a-britain-fit-822 for-the-future.
- 823 [3] R. De Laubier, M. Wunder, S. Witthöft, C. Rothballer, Will 3D printing remodel the construction industry, Boston, MA: The Boston Consulting Group (BCG). (2018).
 825 https://image-src.bcg.com/Images/BCG-Will-3D-Printing-Remodel-the-Construction826 Industry-Jan-2018 tcm9-181569.pdf.
- T. Wangler, R.J. Flatt, First RILEM International Conference on Concrete and Digital Fabrication—Digital Concrete 2018, RILEM Bookseries Vol.19, Springer, 2018.
- [5] F.P. Bos, S.S. Lucas, R.J.M. Wolfs, T.A. Salet, Second RILEM International Conference
 on Concrete and Digital Fabrication: Digital Concrete 2020, RILEM Bookseries Vol.28,
 Springer Nature, 2020.
- J. Dils, V. Boel, G. De Schutter, Influence of cement type and mixing pressure on air content, rheology and mechanical properties of UHPC, Construction and Building Materials. 41 (2013) 455–463. https://doi.org/10.1016/j.conbuildmat.2012.12.050.
- J. Dils, G. De Schutter, V. Boel, Influence of mixing procedure and mixer type on fresh and hardened properties of concrete: a review, Materials and Structures. 45 (2012) 1673–1683. https://doi.org/10.1617/s11527-012-9864-8.
- 838 [8] A. Vandenberg, H. Bessaies-Bey, K. Wille, N. Roussel, Enhancing Printable Concrete 839 Thixotropy by High Shear Mixing, in: Wangler T., Flatt R. (Eds) First RILEM 840 International Conference on Concrete and Digital Fabrication – Digital Concrete 2018. 841 DC 2018. RILEM Bookseries, Springer, 2018: pp. 94–101. https://doi.org/10.1007/978-842 3-319-99519-9_9.
- V. Mechtcherine, F.P. Bos, A. Perrot, W.R.L. da Silva, V.N. Nerella, S. Fataei, R.J.M. Wolfs, M. Sonebi, N. Roussel, Extrusion-based additive manufacturing with cement-based materials Production steps, processes, and their underlying physics: A review, Cement and Concrete Research. 132 (2020) 106037. https://doi.org/10.1016/j.cemconres.2020.106037.
- [10] D. Marchon, S. Kawashima, H. Bessaies-Bey, S. Mantellato, S. Ng, Hydration and rheology control of concrete for digital fabrication: Potential admixtures and cement chemistry, Cement and Concrete Research. 112 (2018) 96–110. https://doi.org/10.1016/j.cemconres.2018.05.014.
- [11] T. Wangler, F. Scotto, E. Lloret-Fritschi, R.J. Flatt, Residence time distributions in continuous processing of concrete, in: Mechtcherine V., Khayat K., Secrieru E. (Eds)
 Rheology and Processing of Construction Materials. RheoCon 2019, SCC 2019. RILEM
 Bookseries Vol. 23, Springer, 2019: pp. 448–456.
- 856 [12] D. Chopin, F. de Larrard, B. Cazacliu, Why do HPC and SCC require a longer mixing 857 time?, Cement and Concrete Research. 34 (2004) 2237–2243. 858 https://doi.org/10.1016/j.cemconres.2004.02.012.

- 859 [13] B. Cazacliu, In-mixer measurements for describing mixture evolution during concrete 860 mixing, Chemical Engineering Research and Design. 86 (2008) 1423–1433. 861 https://doi.org/10.1016/j.cherd.2008.08.021.
- 862 [14] P.-H. Jézéquel, V. Collin, Mixing of concrete or mortars: dispersive aspects, Cement and Concrete Research. 37 (2007) 1321–1333. https://doi.org/DOI: 10.1016/j.cemconres.2007.05.007.
- 865 [15] D. Kaplan, F. de Larrard, T. Sedran, Design of Concrete Pumping Circuit, ACI Materials Journal. 102 (2005) 110–117.
- 867 [16] K. Kasten, Gleitrohr Rheometer, Ein Verfahren zur Bestimmung der Fließeigenschaften 868 von Dickstoffen in Rohrleitungen [in German], in: PHD Thesis, TU Dresden, 2010.
- 869 [17] S. Jo, C. Park, J. Jeong, S. Lee, S. Kwon, A Computational Approach to Estimating a 870 Lubricating Layer in Concrete Pumping, Computers, Materials and Continua. 27 (2012) 871 189–210.
- 872 [18] G. De Schutter, D. Feys, Pumping of fresh concrete: insights and challenges, RILEM 873 Technical Letters. 1 (2016) 76–80. https://doi.org/DOI: https://doi.org/10.21809/rilemtechlett.2016.15.
- 875 [19] V. Mechtcherine, V.N. Nerella, K. Kasten, Testing pumpability of concrete using Sliding 876 Pipe Rheometer, Construction and Building Materials. 53 (2014) 312–323. 877 https://doi.org/10.1016/j.conbuildmat.2013.11.037.
- 878 [20] E. Secrieru, W. Mohamed, S. Fataei, V. Mechtcherine, Assessment and prediction of concrete flow and pumping pressure in pipeline, Cement and Concrete Composites. 107 (2020) 103495. https://doi.org/10.1016/j.cemconcomp.2019.103495.
- 881 [21] E. Secrieru, Pumping behaviour of modern concretes—Characterisation and prediction, 882 PhD Thesis, TU Dresden, 2018.
- 883 [22] N. Roussel, Rheological requirements for printable concretes, Cement and Concrete Research. 112 (2018) 76–85. https://doi.org/10.1016/j.cemconres.2018.04.005.
- 885 [23] D. Kaplan, Pompage des bétons, PhD thesis, Ecole Nationale des Ponts et Chaussées, 886 2000.
- 887 [24] S.H. Kwon, K.P. Jang, J.H. Kim, S.P. Shah, State of the art on prediction of concrete 888 pumping, International Journal of Concrete Structures and Materials. 10 (2016) 75–85. 889 https://doi.org/10.1007/s40069-016-0150-y.
- 890 [25] S.H. Kwon, C.K. Park, J.H. Jeong, S.D. Jo, S.H. Lee, Prediction of concrete pumping: 891 Part II-Analytical prediction and experimental verification, ACI Materials Journal. 110 892 (2013) 657.
- 893 [26] S.H. Kwon, C.K. Park, J.H. Jeong, S.D. Jo, S.H. Lee, Prediction of Concrete Pumping: 894 Part I--Development of New Tribometer for Analysis of Lubricating Layer., ACI 895 Materials Journal. 110 (2013).
- 896 [27] M.S. Choi, Y.J. Kim, J.K. Kim, Prediction of Concrete Pumping Using Various 897 Rheological Models, International Journal of Concrete Structures and Materials. 8 (2014) 898 269–278. https://doi.org/10.1007/s40069-014-0084-1.
- [28] D. Feys, K.H. Khayat, R. Khatib, How do concrete rheology, tribology, flow rate and pipe radius influence pumping pressure?, Cement and Concrete Composites. 66 (2016) 38–46. https://doi.org/10.1016/j.cemconcomp.2015.11.002.
- 902 [29] R.A. Basterfield, C.J. Lawrence, M.J. Adams, On the interpretation of orifice extrusion data for viscoplastic materials, Chemical Engineering Science. 60 (2005) 2599–2607. https://doi.org/10.1016/j.ces.2004.12.019.
- 905 [30] A. Perrot, D. Rangeard, N. Venkatesh, V. Mechtcherine, Extrusion of cement-based 906 materials - an overview, RILEM Technical Letters. 3 (2019). 907 https://doi.org/10.21809/rilemtechlett.2018.75.

- 908 [31] X. Zhou, Z. Li, M. Fan, H. Chen, Rheology of semi-solid fresh cement pastes and mortars 909 in orifice extrusion, Cement and Concrete Composites. 37 (2013) 304–311. 910 https://doi.org/10.1016/j.cemconcomp.2013.01.004.
- 911 [32] X. Zhou, Z. Li, Characterization of rheology of fresh fiber reinforced cementitious 912 composites through ram extrusion, Materials and Structures. 38 (2005) 17–24. 913 https://doi.org/10.1007/BF02480570.
- 914 [33] A. Perrot, Y. Mélinge, D. Rangeard, F. Micaelli, P. Estellé, C. Lanos, Use of ram extruder 915 as a combined rheo-tribometer to study the behaviour of high yield stress fluids at low 916 strain rate, Rheologica Acta. 51 (2012) 743–754. https://doi.org/10.1007/s00397-012-917 0638-6.
- 918 [34] G.L. Guerrini, R. Alfani, Rheological characterisation of cement-based compositions for the extrusion technology, in: Cement Combinations for Durable Concrete: Proceedings of the International Conference Held at the University of Dundee, Scotland, UK. Thomas Telford Publishing., 2005: pp. 81–90. http://www.icevirtuallibrary.com/doi/abs/10.1680/ccfdc.34013.0009.
- 923 [35] F. Micaelli, C. Lanos, G. Levita, Rheology and Extrusion of Cement-Fly Ashes Pastes, in: 924 AIP Conference Proceedings, AIP, 2008: pp. 665–667.
- 925 [36] R. Alfani, N. Grizzuti, G.L. Guerrini, G. Lezzi, The use of the capillary rheometer for the 926 rheological evaluation of extrudable cement-based materials, Rheologica Acta. 46 (2007) 927 703–709. https://doi.org/10.1007/s00397-007-0164-0.
- 928 [37] R. Alfani, G.L. Guerrini, Rheological test methods for the characterization of extrudable cement-based materials—a review, Materials and Structures. 38 (2005) 239–247. 930 https://doi.org/10.1007/BF02479349.
- 931 [38] S.A. Nair, H. Alghamdi, A. Arora, I. Mehdipour, G. Sant, N. Neithalath, Linking fresh paste microstructure, rheology and extrusion characteristics of cementitious binders for 3D printing, Journal of the American Ceramic Society. 102 (2019) 3951–3964. https://doi.org/10.1111/jace.16305.
- 935 [39] S.A. Nair, S. Panda, M. Santhanam, G. Sant, N. Neithalath, A critical examination of the influence of material characteristics and extruder geometry on 3D printing of cementitious binders, Cement and Concrete Composites. (2020) 103671. https://doi.org/10.1016/j.cemconcomp.2020.103671.
- 939 [40] V.N. Nerella, Development and characterisation of cement-based materials for extrusion-940 based 3D-printing, PhD Thesis, TU Dresden, 2020.
- 941 [41] P. Pessoa, E. Paladino, J. Lima, A simplified model for the flow in a progressive cavity pump, in: 20th International Congress of Mechanical Engineering, Brazil, 2009.
- 943 [42] A. Perrot, D. Rangeard, Y. Mélinge, Prediction of the ram extrusion force of cement-based 944 materials, Applied Rheology. 24 (2014) 53320. https://doi.org/DOI: 945 10.3933/APPLRHEOL-24-53320.
- 946 [43] A. Perrot, C. Lanos, Y. Melinge, P. Estellé, Mortar physical properties evolution in extrusion flow, Rheologica Acta. 46 (2007) 1065–1073. https://doi.org/10.1007/s00397-007-0195-6.
- 949 [44] K. El Cheikh, S. Rémond, N. Khalil, G. Aouad, Numerical and experimental studies of 950 aggregate blocking in mortar extrusion, Construction and Building Materials. 145 (2017) 951 452–463. https://doi.org/10.1016/j.conbuildmat.2017.04.032.
- 952 [45] A. Perrot, 3D Printing of Concrete: State of the Art and Challenges of the Digital Construction Revolution, John Wiley&Sons, Wiley-ISTE, 2019.
- 954 [46] C. Ancey, S. Cochard, The dam-break problem for Herschel–Bulkley viscoplastic fluids 955 down steep flumes, Journal of Non-Newtonian Fluid Mechanics. 158 (2009) 18–35. 956 https://doi.org/DOI: 10.1016/j.jnnfm.2008.08.008.
- 957 [47] A. Pierre, P. Estellé, C. Lanos, Extension of spread-slump formulae for yield stress evaluation, Applied Rheology. (2013) 63849.

- 959 [48] P. Coussot, Rheometry of pastes, suspensions, and granular materials: applications in industry and environment, John Wiley & Sons, 2005.
- [49] P. Carneau, R. Mesnil, N. Ducoulombier, N. Roussel, O. Baverel, Characterisation of the
 Layer Pressing Strategy for Concrete 3D Printing, in: Second RILEM International
 Conference on Concrete and Digital Fabrication: Digital Concrete 2020, RILEM
 Bookseries Vol.28, Springer Nature, 2020: pp. 185–195.
- 965 [50] S. Lim, R.A. Buswell, T.T. Le, S.A. Austin, A.G.F. Gibb, T. Thorpe, Developments in construction-scale additive manufacturing processes, Automation in Construction. 21 (2012) 262–268. https://doi.org/10.1016/j.autcon.2011.06.010.
- 968 [51] N. Roussel, P. Coussot, "Fifty-cent rheometer" for yield stress measurements: From slump 969 to spreading flow, Journal of Rheology. 49 (2005) 705–718. 970 http://dx.doi.org/10.1122/1.1879041.
- 971 [52] N. Roussel, The LCPC BOX: a cheap and simple technique for yield stress measurements 972 of SCC, Materials and Structures. 40 (2007) 889–896. https://doi.org/10.1617/s11527-973 007-9230-4.

975

976

980

981

982

986

987

- [53] T.L.H. Nguyen, N. Roussel, P. Coussot, Correlation between L-box test and rheological parameters of a homogeneous yield stress fluid, Cement and Concrete Research. 36 (2006) 1789–1796. https://doi.org/10.1016/j.cemconres.2006.05.001.
- 977 [54] R.J.M. Wolfs, F.P. Bos, T.A.M. Salet, Early age mechanical behaviour of 3D printed 978 concrete: Numerical modelling and experimental testing, Cement and Concrete Research. 979 106 (2018) 103–116. https://doi.org/10.1016/j.cemconres.2018.02.001.
 - [55] A. Suiker, Mechanical performance of wall structures in 3D printing processes: Theory, design tools and experiments, International Journal of Mechanical Sciences. 137 (2018) 145–170. https://doi.org/10.1016/j.ijmecsci.2018.01.010.
- 983 [56] A.S.J. Suiker, R.J.M. Wolfs, S.M. Lucas, T.A.M. Salet, Elastic buckling and plastic 984 collapse during 3D concrete printing, Cement and Concrete Research. 135 (2020) 106016. 985 https://doi.org/10.1016/j.cemconres.2020.106016.
 - [57] J. Kruger, S. Zeranka, G. van Zijl, 3D concrete printing: a lower bound analytical model for buildability performance quantification, Automation in Construction. 106 (2019) 102904. https://doi.org/ttps://doi.org/10.1016/j.autcon.2019.102904.
- 989 [58] N. Roussel, J. Spangenberg, J. Wallevik, R. Wolfs, Numerical simulations of concrete 990 processing: from standard formative casting to additive manufacturing, Cement and 991 Concrete Research. 135 (2020) 106075. 992 https://doi.org/10.1016/j.cemconres.2020.106075.
- [59] L. Reiter, T. Wangler, N. Roussel, R.J. Flatt, The role of early age structural build-up in digital fabrication with concrete, Cement and Concrete Research. 112 (2018) 86–95.
 https://doi.org/10.1016/j.cemconres.2018.05.011.
- 996 [60] N. Roussel, A thixotropy model for fresh fluid concretes: Theory, validation and 997 applications, Cement and Concrete Research. 36 (2006) 1797–1806. http://dx.doi.org/10.1016/j.cemconres.2006.05.025.
- 999 [61] A. Perrot, A. Pierre, S. Vitaloni, V. Picandet, Prediction of lateral form pressure exerted by concrete at low casting rates, Materials and Structures. 48 (2015) 2315–2322. https://doi.org/10.1617/s11527-014-0313-8.
- 1002 [62] T. Lecompte, A. Perrot, Non-linear modeling of yield stress increase due to SCC structural 1003 build-up at rest, Cement and Concrete Research. 92 (2017) 92–97. https://doi.org/10.1016/j.cemconres.2016.11.020.
- [63] J. Kruger, S. Zeranka, G. van Zijl, Quantifying Constructability Performance of 3D
 Concrete Printing via Rheology-Based Analytical Models, in: Mechtcherine V., Khayat
 K., Secrieru E. (Eds) Rheology and Processing of Construction Materials. RheoCon 2019,
 SCC 2019. RILEM Bookseries Vol. 23, Springer, Cham, 2020: pp. 400–408.

- 1009 [64] A. Perrot, D. Rangeard, A. Pierre, Structural built-up of cement-based materials used for 3D-printing extrusion techniques, Materials and Structures. 49 (2016) 1213–1220. https://doi.org/10.1617/s11527-015-0571-0.
- 1012 [65] T. Wangler, E. Lloret, L. Reiter, N. Hack, F. Gramazio, M. Kohler, M. Bernhard, B. Dillenburger, J. Buchli, N. Roussel, R. Flatt, Digital Concrete: Opportunities and 1013 1014 Challenges, **RILEM** Technical Letters; Vol (2016)DO 1015 10.21809/Rilemtechlett.2016.16. (2016).https://letters.rilem.net/index.php/rilem/article/view/16. 1016
- 1017 [66] E. Keita, H. Bessaies-bey, W. Zuo, P. Belin, N. Roussel, Weak bond strength between successive layers in extrusion-based additive manufacturing: measurement and physical origin, Cement and Concrete Research. 123 (2019) 105787. https://doi.org/10.1016/j.cemconres.2019.105787.
- 1021 [67] P. Coussot, Scaling approach of the convective drying of a porous medium, The European Physical Journal B-Condensed Matter and Complex Systems. 15 (2000) 557–566. https://doi.org/10.1007/s100510051160.
- 1024 [68] E. Keita, T.E. Kodger, P. Faure, S. Rodts, D.A. Weitz, P. Coussot, Water retention against drying with soft-particle suspensions in porous media, Physical Review E. 94 (2016) 033104. https://doi.org/10.1103/PhysRevE.94.033104.
- 1027 [69] E. Keita, Y. Rifaai, P. Belin, N. Roussel, Influence of non-adsorbing polymers on drying of fresh mortars, Cement and Concrete Research. 116 (2019) 38–44. https://doi.org/10.1016/j.cemconres.2018.10.016.
- 1030 [70] E. Keita, P. Faure, S. Rodts, P. Coussot, MRI evidence for a receding-front effect in drying porous media, Physical Review E. 87 (2013) 062303. https://doi.org/10.1103/PhysRevE.87.062303.
- 1033 [71] V. Slowik, M. Schmidt, R. Fritzsch, Capillary pressure in fresh cement-based materials and identification of the air entry value, Cement and Concrete Composites. 30 (2008) 557– 565. https://doi.org/10.1016/j.cemconcomp.2008.03.002.
- 1036 [72] V. Picandet, D. Rangeard, A. Perrot, T. Lecompte, Permeability measurement of fresh cement paste, Cement and Concrete Research. 41 (2011) 330–338. https://doi.org/10.1016/j.cemconres.2010.11.019.
- 1039 [73] A. Perrot, D. Rangeard, V. Picandet, S. Serhal, Effect of coarse particle volume fraction on the hydraulic conductivity of fresh cement based material, Materials and Structures. 48 (2015) 2291–2297. https://doi.org/10.1617/s11527-014-0311-x.
- 1042 [74] P.K. Mehta, P.J. Monteiro, Concrete microstructure, properties and materials, McGraw-1043 Hill Education, 2017.
- 1044 [75] N. Burlion, F. Bourgeois, J.F. Shao, Coupling damage-drying shrinkage: experimental study and modelling, in: Proceedings of the International RILEM Workshop on Shrinkage of Concrete, 2000: pp. 703–727.
- 1047 [76] Z.P. Bazant, Mathematical modeling of creep and shrinkage of concrete, Wiley, 1988.
- 1048 [77] Y. Xu, Experimental Study of ABS Material Shrinkage and Deformation Based on Fused 1049 Deposition Modeling, MATEC Web Conf. 67 (2016) 03039. 1050 https://doi.org/10.1051/matecconf/20166703039.
- 1051 [78] J.-H. Jeong, J.-S. Lim, R.-J. Sun, D.G. Zollinger, Modelling of differential shrinkage of pavement slabs, Proceedings of the Institution of Civil Engineers Transport. 165 (2012) 3–14. https://doi.org/10.1680/tran.10.00020.
- [79] American Concrete Institute, ACI Committee 209--Creep and Shrinkage, eds., Guide for
 modeling and calculating shrinkage and creep in hardened concrete, American Concrete
 Institute, Farmington Hills, MI, 2008.
- 1057 [80] V. Gribniak, G. Kaklauskas, D. Bacinskas, Shrinkage in reinforced concrete structures: A computational aspect, Journal of Civil Engineering and Management. 14 (2008) 49–60. https://doi.org/10.3846/1392-3730.2008.14.49-60.

- 1060 [81] Z.P. Bažant, J.-K. Kim, Consequences of diffusion theory for shrinkage of concrete, 1061 Materials and Structures. 24 (1991) 323–326. https://doi.org/10.1007/BF02472065.
- 1062 [82] P. Chen, W. Zheng, Y. Wang, W. Chang, Analysis and Modelling of Shrinkage and Creep 1063 of Reactive Powder Concrete, Applied Sciences. 8 (2018) 732. 1064 https://doi.org/10.3390/app8050732.
- 1065 [83] M. Luković, B. Šavija, E. Schlangen, G. Ye, K. Van Breugel, A 3D Lattice Modelling 1066 Study of Drying Shrinkage Damage in Concrete Repair Systems, Materials. 9 (2016) 575. 1067 https://doi.org/10.3390/ma9070575.
- 1068 [84] D. Gawin, F. Pesavento, B.A. Schrefler, Modelling creep and shrinkage of concrete by 1069 means of effective stresses, Mater Struct. 40 (2007) 579–591. https://doi.org/10.1617/s11527-006-9165-1.
- 1071 [85] D.P. Bentz, D.A. Quenard, V. Baroghel-Bouny, E.J. Garboczi, H.M. Jennings, Modelling drying shrinkage of cement paste and mortar Part 1. Structural models from nanometres to millimetres, Materials and Structures. 28 (1995) 450–458. https://doi.org/10.1007/BF02473164.
- 1075 [86] M. Rezvani, T. Proske, C.-A. Graubner, Modelling the drying shrinkage of concrete made with limestone-rich cements, Cement and Concrete Research. 115 (2019) 160–175. https://doi.org/10.1016/j.cemconres.2018.09.003.
- 1078 [87] L. Granger, J.-M. Torrenti, P. Acker, Thoughts about drying shrinkage: Scale effects and modelling, Mat. Struct. 30 (1997) 96–105. https://doi.org/10.1007/BF02486310.
- 1080 [88] M. Asad, Computational Modelling of shrinkage in repaired concrete, KFUPM, 1995.

- 1081 [89] R. Mu, J.P. Forth, Modelling shrinkage of concrete from moisture lost using moisture 1082 diffusion theory, Magazine of Concrete Research. 61 (2009) 491–497. https://doi.org/10.1680/macr.2008.00105.
 - [90] A.E. Idiart, C.M. López, I. Carol, Modeling of drying shrinkage of concrete specimens at the meso-level, Mater Struct. 44 (2011) 415–435. https://doi.org/10.1617/s11527-010-9636-2.
- 1087 [91] W.P. Boshoff, R. Combrinck, Modelling the severity of plastic shrinkage cracking in concrete, Cement and Concrete Research. 48 (2013) 34–39. https://doi.org/10.1016/j.cemconres.2013.02.003.
- 1090 [92] F. Sayahi, M. Emborg, H. Hedlund, A. Cwirzen, M. Stelmarczyk, The severity of plastic 1091 shrinkage cracking in concrete: A new model, Magazine of Concrete Research. (2019) 1– 1092 10.
- 1093 [93] J. Liu, Q. Tian, C. Miao, Investigation on the plastic shrinkage of cementitious materials under drying conditions: mechanism and theoretical model, Magazine of Concrete Research. 64 (2012) 551–561. https://doi.org/10.1680/macr.11.00037.
- 1096 [94] S. Ghourchian, M. Wyrzykowski, M. Plamondon, P. Lura, On the mechanism of plastic shrinkage cracking in fresh cementitious materials, Cement and Concrete Research. 115 (2019) 251–263. https://doi.org/10.1016/j.cemconres.2018.10.015.
- 1099 [95] J.E. Wallevik, O.H. Wallevik, Concrete mixing truck as a rheometer, Cement and 1100 Concrete Research. 127 (2020) 105930. https://doi.org/10.1016/j.cemconres.2019.105930.
- 1102 [96] V. Mechtcherine, A. Gram, K. Krenzer, J.-H. Schwabe, S. Shyshko, N. Roussel, Simulation of fresh concrete flow using Discrete Element Method (DEM): theory and applications, Materials and Structures. 47 (2014) 615–630.
- 1105 [97] N. Roussel, A. Gram, Simulation of fresh concrete flow, State-of-the Art Report of the RILEM Technical Committee 222-SCF, Volume 15, Springer, 2014.
- 1107 [98] P.A. Cundall, R.D. Hart, Numerical modelling of discontinua, Engineering Computations. 9 (1992) 101–113.
- 1109 [99] H. Chu, A. Machida, N. Suzuki, Experimental investigation and DEM simulation of filling capacity of fresh concrete, Transactions of the Japan Concrete Institute. 18 (1997) 9–14.

- 1111 [100] H. Chu, A. Machida, Numerical simulation of fluidity behavior of fresh concrete by 2D distincg element method, Transactions of the Japan Concrete Institute. 18 (1997) 1–8.
- 1113 [101] V. Mechtcherine, S. Shyshko, Simulating the behaviour of fresh concrete with the
 1114 Distinct Element Method Deriving model parameters related to the yield stress, Cement
 1115 and Concrete Composites. 55 (2015) 81–90.
 1116 https://doi.org/10.1016/j.cemconcomp.2014.08.004.
- 1117 [102] R. Deng, Y. Tan, H. Zhang, X. Xiao, S. Jiang, Experimental and DEM studies on the 1118 transition of axial segregation in a truck mixer, Powder Technology. 314 (2017) 148–163. 1119 https://doi.org/10.1016/j.powtec.2016.08.013.
- 1120 [103] Y. Tan, G. Cao, H. Zhang, J. Wang, R. Deng, X. Xiao, B. Wu, Study on the Thixotropy 1121 of the Fresh Concrete Using DEM, Procedia Engineering. 102 (2015) 1944–1950. 1122 https://doi.org/10.1016/j.proeng.2015.06.138.
- [104] K. Krenzer, V. Mechtcherine, U. Palzer, Simulating mixing processes of fresh concrete using the discrete element method (DEM) under consideration of water addition and changes in moisture distribution, Cement and Concrete Research. 115 (2019) 274–282. https://doi.org/10.1016/j.cemconres.2018.05.012.
- 1127 [105] M. Choi, N. Roussel, Y. Kim, J. Kim, Lubrication layer properties during concrete 1128 pumping, Cement and Concrete Research. 45 (2013) 69–78. 1129 https://doi.org/10.1016/j.cemconres.2012.11.001.
- 1130 [106] M.S. Choi, Y.J. Kim, S.H. Kwon, Prediction on pipe flow of pumped concrete based on shear-induced particle migration, Cement and Concrete Research. 52 (2013) 216–224. https://doi.org/10.1016/j.cemconres.2013.07.004.
- 1133 [107] L. Chen, G. Liu, W. Cheng, G. Pan, Pipe flow of pumping wet shotcrete based on lubrication layer, SpringerPlus. 5 (2016) 945. https://doi.org/10.1186/s40064-016-2633-1135 3.
- [108] Y. Tan, H. Zhang, D. Yang, S. Jiang, J. Song, Y. Sheng, Numerical simulation of concrete pumping process and investigation of wear mechanism of the piping wall, Tribology International. 46 (2012) 137–144. https://doi.org/10.1016/j.triboint.2011.06.005.
- 1140 [109] V.N. Nerella, V. Mechtcherine, Virtual Sliding Pipe Rheometer for estimating pumpability of concrete, Construction and Building Materials. 170 (2018) 366–377. https://doi.org/10.1016/j.conbuildmat.2018.03.003.
- 1143 [110] G. De Schutter, Thixotropic effects during large-scale concrete pump tests on site, in:
 1144 Advances in Construction Materials and Systems (ICACMS), Vol. 2, RILEM
 1145 Publications, 2017: pp. 1–7.
- 1146 [111] R. De Schryver, K. El Cheikh, M.Y. Yardimci, K. Lesage, G. De Schutter, Fresh
 1147 Concrete Pumping Arrest Investigation for Thixotropy by a CFD Modelling Approach,
 1148 in: Mechtcherine V., Khayat K., Secrieru E. (Eds) Rheology and Processing of
 1149 Construction Materials. RheoCon 2019, SCC 2019. RILEM Bookseries Vol. 23, Springer,
 1150 Cham, 2019: pp. 580–587.
- 1151 [112] S. Remond, P. Pizette, A DEM hard-core soft-shell model for the simulation of concrete 1152 flow, Cement and Concrete Research. 58 (2014) 169–178. 1153 https://doi.org/10.1016/j.cemconres.2014.01.022.
- 1154 [113] R. Jayathilakage, J. Sanjayan, P. Rajeev, Characterizing Extrudability for 3D Concrete 1155 Printing Using Discrete Element Simulations, in: Springer, 2020: pp. 290–300.
- 1156 [114] P. Yang, S.K.A.O. Nair, N. Neithalath, Discrete Element Simulations of Rheological 1157 Response of Cementitious Binders as Applied to 3D Printing, in: T. Wangler, R.J. Flatt 1158 (Eds.), First RILEM International Conference on Concrete and Digital Fabrication – 1159 Digital Concrete 2018, Springer, Cham, 2019: pp. 102–112.
- 1160 [115] H. Khelifi, A. Perrot, T. Lecompte, D. Rangeard, G. Ausias, Prediction of extrusion load 1161 and liquid phase filtration during ram extrusion of high solid volume fraction pastes,

- 1162 Powder Technology. 249 (2013) 258–268. 1163 http://dx.doi.org/10.1016/j.powtec.2013.08.023.
- 1164 [116] E.J. O'Donovan, R.I. Tanner, Numerical study of the Bingham squeeze film problem, 1165 Journal of Non-Newtonian Fluid Mechanics. 15 (1984) 75–83.
- 1166 [117] G.G. Lipscomb, M.M. Denn, Flow of Bingham fluids in complex geometries, Journal of Non-Newtonian Fluid Mechanics. 14 (1984) 337–346.
- 1168 [118] T.C. Papanastasiou, Flows of materials with yield, Journal of Rheology. 31 (1987) 385–1169 404.
- 1170 [119] P.J. Carreau, Rheological equations from molecular network theories, Transactions of the Society of Rheology. 16 (1972) 99–127.
- 1172 [120] R.A. Buswell, W.R. Leal de Silva, S.Z. Jones, J. Dirrenberger, 3D printing using concrete extrusion: A roadmap for research, Cement and Concrete Research. 112 (2018) 37–49. https://doi.org/10.1016/j.cemconres.2018.05.006.
- 1175 [121] A. Pierre, A. Perrot, A. Histace, S. Gharsalli, E. Kadri, A study on the limitations of a vane rheometer for mineral suspensions using image processing, Rheologica Acta. 56 (2017) 351–367. https://doi.org/10.1007/s00397-017-0993-4.

1180

1181

1182 1183

1184

1185 1186

1187 1188

1189

1190

1191

1192

1193

1194

1195 1196

1197

1198

1199

1200 1201

1202 1203

1208

- [122] R.J.M. Wolfs, F.P. Bos, T.A.M. Salet, Triaxial compression testing on early age concrete for numerical analysis of 3D concrete printing, Cement and Concrete Composites. (2019) 103344. https://doi.org/10.1016/j.cemconcomp.2019.103344.
- [123] R. Comminal, M.P. Serdeczny, N. Ranjbar, M. Mehrali, D.B. Pedersen, H. Stang, J. Spangenberg, Modelling of material deposition in big area additive manufacturing and 3D concrete printing, in: Joint Special Interest Group Meeting between Euspen and ASPE Advancing Precision in Additive Manufacturing, The European Society for Precision Engineering and Nanotechnology, 2019: pp. 151–154.
- [124] R. Comminal, W.R.L. da Silva, T.J. Andersen, H. Stang, J. Spangenberg, Influence of Processing Parameters on the Layer Geometry in 3D Concrete Printing: Experiments and Modelling, in: Econd RILEM International Conference on Concrete and Digital Fabrication: Digital Concrete 2020, RILEM Bookseries Vol.28, Springer Nature, Springer, 2020: pp. 852–862.
- [125] R. Comminal, W.R.L. da Silva, T.J. Andersen, H. Stang, J. Spangenberg, Modelling of 3D concrete printing based on computational fluid dynamics, Cement and Concrete Research. 138 (2020) 106256.
- [126] J. Reinold, J.J. Timothy, G. Meschke, Particle finite element simulation for additively manufacturing processes of fresh concrete, Proceedings of the 8th GACM Colloquium on Computational Mechanics for Young Scientists from Academia and Industry, 2019, pp. 339–342., (n.d.).
- [127] Reinold, J.; Nerella, V.N.; Mechtcherine, V.; Meschke, G. Extrusion Process Simulation and Layer Shape Prediction during 3D-Concrete-Printing Using The Particle Finite Element Method. Preprints 2020, 2020070715 (doi: 10.20944/preprints202007.0715.v1), (n.d.).
- [128] R.J.M. Wolfs, T.A.M. Salet, N. Roussel. Filament geometry control in extrusion based additive manufacturing. Journal paper in preparation., (n.d.).
- [129] S. Andersen, W.R.L. da Silva, I. Paegle, J.H. Nielsen, Numerical Model Describing the
 Early Age Behavior of 3D Printed Concrete—Work in Progress, in: Second RILEM
 International Conference on Concrete and Digital Fabrication: Digital Concrete 2020,
 RILEM Bookseries Vol.28, Springer Nature, 2020: pp. 175–184.
 - [130] R. Wolfs, A. Suiker, Structural failure during extrusion-based 3D printing processes, The International Journal of Advanced Manufacturing Technology. 104 (2019) 565–584. https://doi.org/10.1007/s00170-019-03844-6.
- 1211 [131] R.J.M. Wolfs, F.P. Bos, T.A.M. Salet, Correlation between destructive compression tests and non-destructive ultrasonic measurements on early age 3D printed concrete,

- 1213 Construction and Building Materials. 181 (2018) 447–454. 1214 https://doi.org/10.1016/j.conbuildmat.2018.06.060.
- 1215 [132] R. Jayathilakage, P. Rajeev, J.G. Sanjayan, Yield stress criteria to assess the buildability 1216 of 3D concrete printing, Construction and Building Materials. 240 (2020) 117989. 1217 https://doi.org/10.1016/j.conbuildmat.2019.117989.
- 1218 [133] R. Hameed, A. Papon, A. Perrot, Impression 3D en béton-Entre essais physiques et simulations numériques, Béton[s], Le Magazine. (2019).
- 1220 [134] M. Mengesha, A. Schmidt, L. Göbel, T. Lahmer, Numerical Modeling of an Extrusion-1221 Based 3D Concrete Printing Process Considering a Spatially Varying Pseudo-Density 1222 Approach, in: Second RILEM International Conference on Concrete and Digital 1223 Fabrication: Digital Concrete 2020, RILEM Bookseries Vol.28, Springer Nature, 2020: 1224 pp. 323–332.

1226

1227

1228

1236

1237

12381239

1240

1241

1242

1243

1244 1245

1246

1247

1248 1249

1250

1251

- [135] F. Brun, F. Gaspar, A. Mateus, J. Vitorino, F. Diz, Experimental Study on 3D Printing of Concrete with Overhangs, in: Second RILEM International Conference on Concrete and Digital Fabrication: Digital Concrete 2020, RILEM Bookseries Vol.28, Springer Nature, 2020: pp. 778–789.
- [136] R.I. Jayathilakage, P. Rajeev, J. Sanjayan, Predication of strength-based failure in extrusion-based 3D concrete printing, in: Mechtcherine V., Khayat K., Secrieru E. (Eds)
 Rheology and Processing of Construction Materials. RheoCon 2019, SCC 2019. RILEM Bookseries Vol. 23, Springer, Cham, 2019: pp. 391–399.
- 1233 [137] H. Jeong, S.-J. Han, S.-H. Choi, Y.J. Lee, S.T. Yi, K.S. Kim, Rheological property 1234 criteria for buildable 3D printing concrete, Materials. 12 (2019) 657. 1235 https://doi.org/10.3390/ma12040657.
 - [138] Z. Chang, E. Schlangen, B. Šavija, Extended Lattice Model to Simulate the Printing Process of 3D Printed Cementitious Materials, in: Second RILEM International Conference on Concrete and Digital Fabrication: Digital Concrete 2020, RILEM Bookseries Vol.28, Springer Nature, 2020: pp. 814–823.
 - [139] R.J.M. Wolfs, F.P. Bos, E.C.F. Van Strien, T.A.M. Salet, A real-time height measurement and feedback system for 3D concrete printing, in: 2017: pp. 2474–2483. https://doi.org/10.1007/978-3-319-59471-2 282.
 - [140] L. Reiter, T. Wangler, A. Anton, R.J. Flatt, Setting on demand for digital concrete Principles, measurements, chemistry, validation, Cement and Concrete Research. 132 (2020) 106047. https://doi.org/10.1016/j.cemconres.2020.106047.
 - [141] T.T. Le, S.A. Austin, S. Lim, R.A. Buswell, R. Law, A.G. Gibb, T. Thorpe, Hardened properties of high-performance printing concrete, Cement and Concrete Research. 42 (2012) 558–566. https://doi.org/10.1016/j.cemconres.2011.12.003.
 - [142] V.N. Nerella, S. Hempel, V. Mechtcherine, Effects of layer-interface properties on mechanical performance of concrete elements produced by extrusion-based 3D-printing, Construction and Building Materials. 205 (2019) 586–601. https://doi.org/10.1016/j.conbuildmat.2019.01.235.
- 1253 [143] R.J.M. Wolfs, F.P. Bos, T.A.M. Salet, Hardened properties of 3D printed concrete: The influence of process parameters on interlayer adhesion, Cement and Concrete Research. 1255 119 (2019) 132–140. https://doi.org/10.1016/j.cemconres.2019.02.017.
- 1256 [144] S. Ghourchian, M. Wyrzykowski, L. Baquerizo, P. Lura, Susceptibility of Portland cement and blended cement concretes to plastic shrinkage cracking, Cement and Concrete Composites. 85 (2018) 44–55. https://doi.org/10.1016/j.cemconcomp.2017.10.002.
- 1259 [145] C. Schmutzler, T.H. Stiehl, M.F. Zaeh, Empirical process model for shrinkage-induced warpage in 3D printing, RPJ. 25 (2019) 721–727. https://doi.org/10.1108/RPJ-04-2018-0098.

- 1262 [146] H. Wenbin, L. Yong Tsui, G. Haiqing, A study of the staircase effect induced by material shrinkage in rapid prototyping, Rapid Prototyping Journal. 11 (2005) 82–89. https://doi.org/10.1108/13552540510589449.
- 1265 [147] V. Slowik, J.W. Ju, Discrete modeling of plastic cement paste subjected to drying, 1266 Cement and Concrete Composites. 33 (2011) 925–935. https://doi.org/10.1016/j.cemconcomp.2011.02.001.
- 1268 [148] H. Peron, J.Y. Delenne, L. Laloui, M.S. El Youssoufi, Discrete element modelling of drying shrinkage and cracking of soils, Computers and Geotechnics. 36 (2009) 61–69. https://doi.org/10.1016/j.compgeo.2008.04.002.
- 1271 [149] G.S. Slavcheva, Drying and shrinkage of cement paste for 3D printable concrete, IOP Conf. Ser.: Mater. Sci. Eng. 481 (2019) 012043. https://doi.org/10.1088/1757-899X/481/1/012043.
- 1274 [150] L. Hui, F. Lopez Almansa, Experimental Test on Drying Shrinkage of 3D-printed Fiber-1275 reinforced Concrete at Early Ages, AJCEA. 6 (2018) 24–29. 1276 https://doi.org/10.12691/ajcea-6-1-3.
- 1277 [151] K. Federowicz, M. Kaszyńska, A. Zieliński, M. Hoffmann, Effect of Curing Methods 1278 on Shrinkage Development in 3D-Printed Concrete, Materials. 13 (2020) 2590. 1279 https://doi.org/10.3390/ma13112590.
- [152] J. Mago, R. Kumar, R. Agrawal, A. Singh, V. Srivastava, Modeling of Linear Shrinkage
 in PLA Parts Fabricated by 3D Printing Using TOPSIS Method, in: Advances in Additive
 Manufacturing and Joining, Springer, 2020: pp. 267–276.
 - [153] I. Ait-Mansour, N. Kretzschmar, S. Chekurov, M. Salmi, J. Rech, Design-dependent shrinkage compensation modeling and mechanical property targeting of metal FFF, Prog Addit Manuf. 5 (2020) 51–57. https://doi.org/10.1007/s40964-020-00124-8.
- 1286 [154] I. Bahnini, U.K. uz Zaman, M. Rivette, N. Bonnet, A. Siadat, Computer-aided design (CAD) compensation through modeling of shrinkage in additively manufactured parts, Int J Adv Manuf Technol. 106 (2020) 3999–4009. https://doi.org/10.1007/s00170-020-04924-8.
- 1290 [155] U.M. Dilberoglu, S. Simsek, U. Yaman, Shrinkage compensation approach proposed 1291 for ABS material in FDM process, Materials and Manufacturing Processes. 34 (2019) 1292 993–998. https://doi.org/10.1080/10426914.2019.1594252.
- 1293 [156] U. Yaman, Shrinkage compensation of holes via shrinkage of interior structure in FDM process, Int J Adv Manuf Technol. 94 (2018) 2187–2197. https://doi.org/10.1007/s00170-017-1018-2.
- 1296 [157] Q. Huang, J. Zhang, A. Sabbaghi, T. Dasgupta, Optimal offline compensation of shape 1297 shrinkage for three-dimensional printing processes, IIE Transactions. 47 (2015) 431–441. 1298 https://doi.org/10.1080/0740817X.2014.955599.

1283

1284